Tracking the origin of microplastics in the South Atlantic Subtropical Gyre

Arianna Olivelli

Supervisors:

Dr. Erik van Sebille

Dr. Philippe Delandmeter

Dr. Francesca Sangiorgi

Department of Earth Sciences

Utrecht University

Thesis submitted for the degree of

Master of Science

July 2019

Declaration

I hereby declare that except where specific reference is made to the work of others, the contents of this thesis are original and have not been submitted in whole or in part for consideration for any other degree or qualification in this, or any other university. This thesis is my own work and contains nothing which is the outcome of work done in collaboration with others, except as specified in the text and Acknowledgements.

Arianna Olivelli
July 2019

Abstract

Plastic pollution poses one of the most urgent threats of present time to the marine environment. Global plastic production is growing exponentially and causing an unprecedented increase in the amount of mismanaged plastic waste available to enter the world's oceans. Microplastic particles with a density lower than that of seawater float on the ocean surface and tend to accumulate in the Subtropical Gyres of all ocean basins due to geostrophic and Ekman currents and Stokes drift. This work develops a method to analyse the possible pathways followed by particles that were sampled in the South Atlantic Subtropical Gyre in order to identify their sources. To do so, particle trajectories were computed by means of Lagrangian simulations backward in time and for each particle the probability of being sourced from nine selected cities bordering the South Atlantic Ocean was calculated.

Probability calculations were performed following both an exponential and a quadratic modelling approach on two different datasets. Both models were implemented in such a way that the probability decreased with an increase in distance between the particle and the potential source. The probabilities were also a function of the source uncertainty distance, a parameter representing the uncertain distance at which a particle could be identified as being sourced from a given location. The consistency between the results obtained from two modelling approaches and the different datasets allowed to pinpoint the Río de la Plata estuary (comprising Montevideo and Buenos Aires), Cape Town and Rio de Janeiro as the most likely sources of microplastics to the South Atlantic Subtropical Gyre. Additionally, from sensitivity analysis the most meaningful source uncertainty distance was determined to range between 25 and 100 km.

The methodology developed to calculate land source probabilities is fully transferable and could be used regardless of the study domain and the source locations that want to be addressed. For this reason, its simplicity and reliability might make it a powerful tool to identify the relative contribution of different sources and provide a base on which quantitative studies can be performed to assess the amount of microplastics that accumulate in a given region from selected sources.

Layman's Abstract

Plastics have been found in all oceans and their presence poses an urgent threat on wildlife and the ecosystems. Floating plastics tend to accumulate in the middle of the Subtropical Gyres, which are large-scale systems of surface currents. In this study, the pathways followed by microplastics (plastics smaller than 5 mm) in the South Atlantic Ocean were studied from computer simulations.

From the computation of the trajectories of virtual microplastic particles released in the open ocean and tracked backward in time, the probabilities with which nine of the most populous cities on the eastern coast of South America and western coast of Africa are sourcing microplastics to the South Atlantic Subtropical Gyre were calculated. Montevideo, Buenos Aires, Cape Town and Rio de Janeiro resulted to be the cities with the highest probabilities of being the land sources of microplastics among all those assessed. The methodology developed to calculate the probabilities of different land sources could be fully transferred to other ocean basins and/or used to identify other land and ocean sources, making it a powerful tool for future studies aiming to quantify the contribution of various cities and rivers to the pollution of the marine environment.

Contents

List of Figures

List of Tables

1. General Introduction

1.1. Plastic pollution

Marine plastic pollution is one of the most urgent environmental, societal and economic issues of present times. Plastic has been found floating on the water surface (Cózar et al., 2014), accumulating on the seafloor (Woodall et al., 2014) and washing up on shorelines (Galgani et al., 2015) in all ocean basins. It has been observed in polar regions of both hemispheres (Isobe et al., 2017; Obbard et al., 2014) and in some of the most remote areas on the planet (Lavers and Bond, 2017). Plastic in the marine environment has been found to cause biodiversity losses (Derraik, 2002; Gall and Thompson, 2015), to negatively impact the reproduction and development of different wildlife species (Oehlmann et al., 2009) and potentially threat human health (Thompson et al., 2009; Wright and Kelly, 2017).

Global plastic production reached 350 million tonnes in 2015 (Geyer et al., 2017) and is doubling approximately every 11 years (PlasticsEurope, 2013), meaning that the amount of plastics produced between 2019 and 2030 will be the same as that manufactured between 1950, when large scale plastic production began, and 2019. The majority of plastic is produced for packaging purposes (Geyer et al., 2017; PlasticsEurope, 2018), therefore having a short life span and in most cases turning into waste after a single use. The vast amount of discarded single-use plastic is particularly problematic in developing countries, where the consumer capacity is increasing significantly as a consequence of improving economic conditions, while adequate waste management infrastructure is lagging. As a result, the interplay between these two factors will cause an increase in the amount of plastic available to enter the marine environment unless robust waste management policies are implemented in the near future (Jambeck et al., 2015, 2018; Lebreton and Andrady, 2019).

It was estimated that the amount of mismanaged plastic waste available to enter the ocean from coastal areas in 2010 alone ranged from 4.8 to 12.7 million tonnes (Jambeck et al., 2015), while Lebreton et al. (2017) estimated that between 1.51 and 2.41 million tonnes enter the ocean from riverine input every year. While at the moment the most critical region is represented by Asia (Jambeck et al., 2015; Lebreton and Andrady, 2019), Africa's unprecedented population growth and progressive urbanisation in coastal areas, together with the increased consumer capacity of its people and the lag in adequate waste managment infrastucture, have the potential to shift the main hot-spot of land-sourced plastic to the ocean from South-East Asia to Africa as soon as in 2040 (Jambeck et al., 2018; Lebreton and Andrady, 2019).

Based on size, plastic can enter the world's oceans as macroplastic (>5 mm) or microplastic (<5 mm) (Arthur et al., 2009; Frias and Nash, 2019). In this work, due to the use of data gathered and analysed by different studies, the term microplastics refers to all plastic debris collected in surface-trawling plankton nets during surveys (van Sebille et al., 2015). Microplastics can be primarily produced in that size or can be the result of larger debris breaking down due to mechanical and chemical weathering. The former is mainly a consequence of wave action in coastal areas, while the main factors involved in the latter are the exposure to solar ultraviolet (UV) radiation and ambient temperature (Andrady, 2011).

In the open ocean, buoyant plastics were found to accumulate in all five Subtropical Gyres, where smaller fragments are more abundant than larger debris (Cózar et al., 2014; Eriksen et al., 2014). These empirical findings were also reproduced by numerical models, which allowed to quantify the counts and mass of microplastics floating on the ocean surface in the range of 15 to 51 trillion particles and 93 and 236 thousand metric tons, respectively (van Sebille et al., 2015; Lebreton et al., 2012; Maximenko et al., 2012; van Sebille et al., 2012). The accumulation of debris in the Subtropical Gyres is due to the converging dynamics of Ekman currents at mid-latitudes (Maximenko et al., 2012; Onink et al., 2019). As plastics are often less dense than seawater, they do not sink with water in the regions where surface convergence is the strongest and they accumulate on the surface.

1.2. South Atlantic Subtropical Gyre

The Southern Hemisphere is characterised by a scarcity of field measurements of (micro)plastic abundance in the marine environment compared to the Northern Hemisphere, and the South Atlantic Ocean is no exception to this. Nevertheless, plastic debris was found stranded on the uninhabited Inaccessible Island, in the middle of the basin, more than three decades ago (Ryan and Watkins, 1988). While, as previously stated, modelling studies have identified all five Subtropical Gyres to be accumulation areas for plastic debris, more empirical data is needed to quantify the extent of marine plastic pollution to the ocean basins of the Southern Hemisphere.

In addition to the data collected by the two global expeditions presented in Eriksen et al. (2014) and Cózar et al. (2014), microplastics were also found floating in the western tropical region of the South Atlantic (Do Sul et al., 2014) and Ryan

(2014) identified an area of higher debris density between 3 - 8°E at a latitude of 34 - 35°S. The characteristics of the litter found within this area (i.e. absence of short-lived litter that would indicate a local source and the high abundance of items with encrusting biota) suggested that the plastics had been drifting for a long time before reaching the accumulation zone, leading to its denomination as the South Atlantic 'garbage patch'.

1.2.1. Surface circulation

The South Atlantic Subtropical Gyre (SASG) is an anticyclonic system of wind-driven surface currents composed of the westward flowing South Equatorial Current at the northern boundary, the southward flowing Brazil Current at the western boundary, the eastward flowing South Atlantic Current at the southern boundary and the northward flowing Benguela Current at the eastern boundary (Figure 1.1).

The circulation in the SASG, as in all subtropical gyres, is the result of geostrophic and Ekman currents. Geostrophic currents are governed by the balance between surface pressure gradients and Coriolis force and the meridional and zonal components of the velocity can be expressed as:

$$u_g = -\frac{1}{f\rho}\frac{\partial p}{\partial y} \qquad\qquad v_g = \frac{1}{f\rho}\frac{\partial p}{\partial x} \tag{1.1}$$

where $f = 2\Omega cos(\phi)$ is the Coriolis parameter, which depends on the Earth's rate of rotation (Ω) and the latitude at which it is computed (ϕ), and ρ is the density of water. Pressure can also be expressed as $p = p_0 + \rho g\eta$, where p_0 is the atmospheric pressure at the ocean surface, g is the gravitational acceleration and η is sea surface height. Therefore, assuming a constant-density ocean where atmospheric pressure is uniform over the surface, geostrophic velocities are a function of sea surface height and can be rewritten as:

$$u_g = -\frac{g}{f}\frac{\partial \eta}{\partial y} \qquad\qquad v_g = \frac{g}{f}\frac{\partial \eta}{\partial x} \tag{1.2}$$

Ekman currents are resulting from the effect of wind stress over the surface of the ocean and are driven by the balance between wind and Coriolis forces. This wind-driven type of current is present only up to a depth of approximately 50 –100 m in the upper ocean (the so-called Ekman layer) and its velocity is higher at the surface and decreases with depth. The depth of the Ekman layer corresponds to the e-folding depth of the velocity and is:

$$H_e = \sqrt{\frac{2A_v}{f}} \tag{1.3}$$

where A_v is the eddy viscosity. At the ocean surface, water moves at an angle of 45° to the left of the wind direction in the Southern Hemisphere because of Coriolis acceleration. The movement of the upper layer induces an acceleration to the left on the layer below, which will have a lower velocity, until the velocity is zero at the bottom of the Ekman layer. The resulting structure is a spiral and its net transport (Ekman transport) is directed exactly 90° towards the left of the wind direction in the Southern Hemisphere. It can be described as:

$$U_e = \frac{\tau_y}{f\rho} \qquad\qquad V_e = -\frac{\tau_x}{f\rho} \tag{1.4}$$

where τ_y and τ_x are the wind stress in the meridional and zonal direction respectively and ρ is the density of the water. As winds are blowing in different directions depending on the latitude, they produce varying stress on the ocean surface and therefore divergence or convergence of water due to Ekman transport. The Trade winds at low latitudes and the Westerlies at mid-latitudes cause convergence and a doming of sea surface, under which water is downwelled due to the conservation of

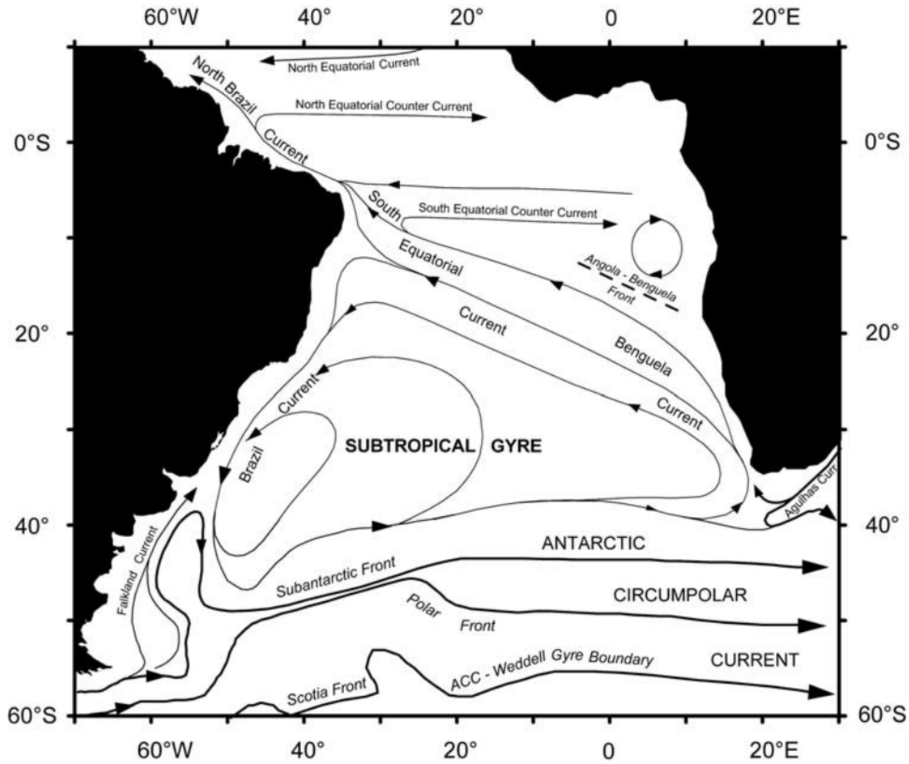

Figure 1.1: Surface circulation in the South Atlantic Ocean. Adapted from Niebler et al. (2003).

mass. As sea surface is higher where Ekman transport converges, this sea surface height difference generates currents that flow around the high pressure area due to geostrophy giving rise to the Subtropical Gyre (Figure 1.2).

1.3. Scope of the project

The South Atlantic Ocean borders only with low and middle income countries, excluding Argentina and Uruguay which are classified as high income (World Bank definitions based on 2017 Gross National Income). In 2015, South American and Western Africa generated almost 10.3 million metric tonnes (Mt) of mismanaged plastic waste (Lebreton and Andrady, 2019) and Brazil and South Africa were among the top twenty countries by generation of mismanaged plastic waste (Jambeck et al., 2015). As mentioned in Section 1.1, Africa even has the potential to become the continent with the highest amount of mismanaged plastic waste by 2040 (Lebreton and Andrady, 2019). For these reasons, assessing the history and fate of plastic pollution in the South Atlantic is extremely relevant and could provide vital information for preventing land waste to enter the marine environment.

This study aims to identify the sources of microplastics floating on the surface

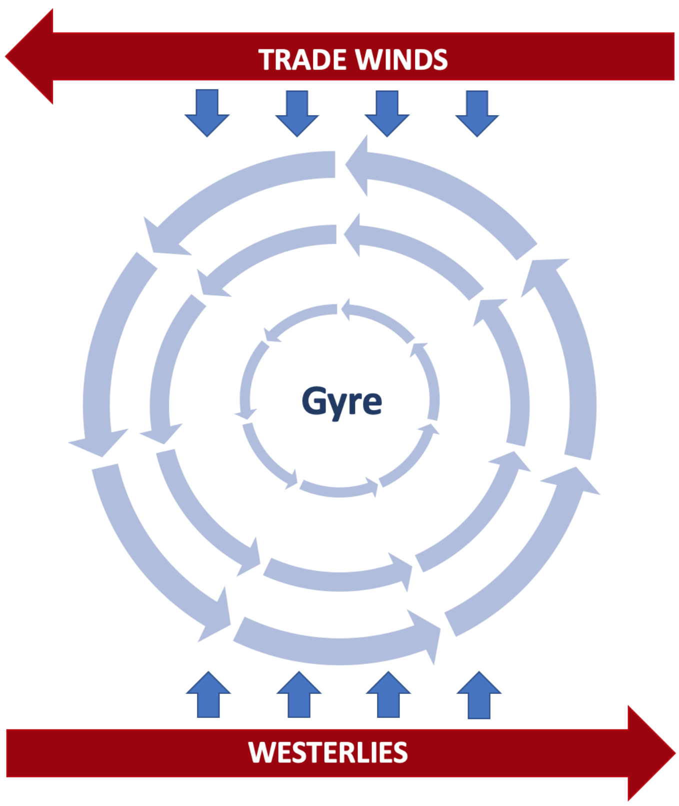

Figure 1.2: Schematic structure of the Subtropical Gyres in the Southern Hemisphere. The small blue arrows represent the direction of Ekman transport. Modified after van Sebille (2015).

layer of the South Atlantic Ocean by means of Lagrangian simulations run backward in time using horizontal general circulation and Stokes drift data for the period between 2005 and 2019 and by the implementation of an innovative algorithm to calculate the probability with which nine of the most populous coastal cities bordering the basin could be the sources of particles accumulating in the SASG. Using data from the Royal Netherlands Institute for Sea Research (NIOZ) 'South Atlantic Subtropical Gyre Plastics Cruise' and from van Sebille et al. (2015), the pathways followed by microplastics collected in the SASG were assessed to identify the most probable land sources. The identification of land sources could give important information on the assemblages of (micro)organisms found on microplastics retrieved during sampling in the field, as particles with different histories have visited different ecosystems within the ocean domain. This is especially relevant for the data obtained from the NIOZ 'South Atlantic Subtropical Gyre Plastics Cruise' expedition, on which further work will be conducted to investigate the assemblages of (micro)organisms colonising microplastic samples.

In Chapter 2, the methods, results and discussion of Lagrangian modelling are presented, providing information on the choices made before the advection of those particles on which probability calculations are made. Chapter 3 contains the methods, results and discussion related to identification of land sources of microplastic to the SASG. The conclusions of the work presented in this thesis are found in Chapter 4.

2. Lagrangian modelling

2.1. Introduction

The pathways or trajectories of microplastic particles on the surface of the South Atlantic Ocean were assessed using a Lagrangian modelling approach. The Lagrangian approach is based on the description of the surrounding environment using a reference frame that moves together with the infinitesimal particle that is being advected and it is considered to be complementary to the Eulerian approach, which is based on the description of fluid dynamics in a fixed reference frame.

Lagrangian modelling consists in the advection backward or forward in time of virtual particles integrated within time-evolving, two- or three-dimensional Eulerian velocity fields often obtained from ocean general circulation models (OGCMs) or from altimetry measurements (van Sebille et al., 2018). While here this approach was used to study microplastic particles, it has to be noted that the applications of Lagrangian modelling in physical oceanography are diverse and for example it has been used to model dispersal of oil spills (North et al., 2011), fish larvae (Lett et al., 2008), sea ice (Lindsay and Stern, 2004; Rampal et al., 2016) and tracers such as nutrients (Chenillat et al., 2015).

2.2. Methods

2.2.1. Field data

Between the 4th and 24th of January 2019 the Royal Netherlands Institute for Sea Research (NIOZ) carried out the 'South Atlantic Subtropical Gyre Plastics Cruise', leaving from Cape Town (South Africa) and heading towards the centre of the South Atlantic Subtropical Gyre. During the expedition surface trawls with manta nets were undertaken at 24 different locations in the eastern part of the South Atlantic Ocean (Figure 2.1; Table 2.1). Microplastics were found at all sampling locations, with a density varying between $6 \cdot 10^2$ and $3.8 \cdot 10^5$ particles/km^2 (mean = $9.6 \cdot 10^4$ particles/km^2; median = $4.3 \cdot 10^4$ particles/km^2). In addition to the data collected during the NIOZ 2019 expedition, field data for the South Atlantic collected by Cózar et al. (2014) and Eriksen et al. (2014) and used in van Sebille et al. (2015)

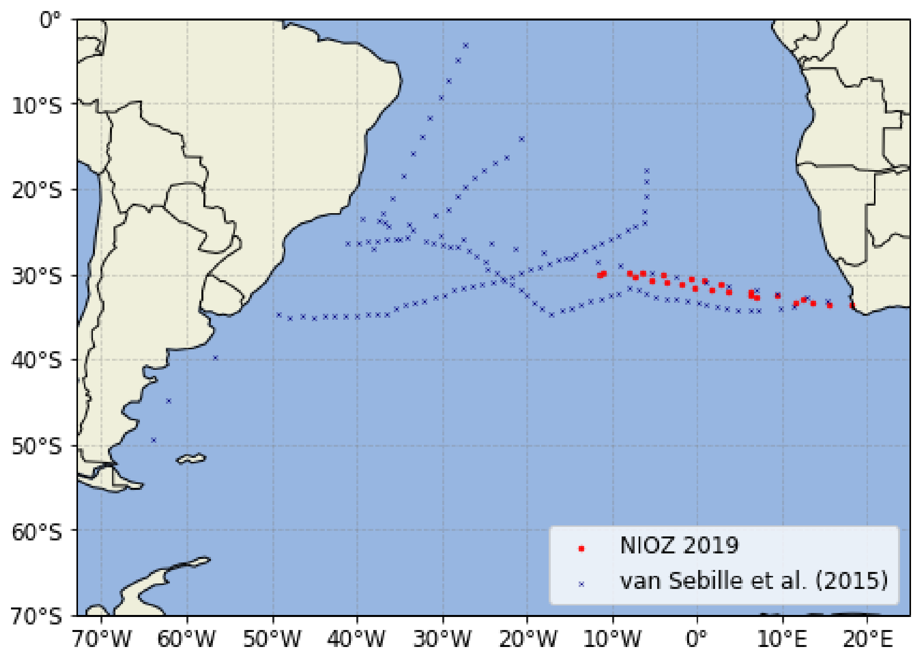

Figure 2.1: Surface trawl sampling locations for the NIOZ 'South Atlantic Subtropical Gyre Plastics Cruise' and previous expeditions considered in van Sebille et al. (2015).

were utilised for part of the simulations and analyses as well.

2.2.2. The Parcels framework

Virtual microplastic particles were advected in a two-dimensional ocean flow field using Parcels (Probably A Really Computationally Efficient Lagrangian Simulator), which is explained in detail in Lange and van Sebille (2017) and Delandmeter and van Sebille (2019). In Parcels, virtual particles advected within the ocean flow field could be prescribed a specific particle 'behaviour', which is expressed by the user in entirely customizable 'kernels'. The trajectory followed by a particle is computed solving the following equation:

$$\boldsymbol{X}(t+\Delta t) = \boldsymbol{X}(t) + \int_{t}^{t+\Delta t} \boldsymbol{v}(\boldsymbol{x},\tau)d\tau + \Delta \boldsymbol{X}_b(t) \tag{2.1}$$

where $\boldsymbol{X}(t)$ is the two-dimensional position of the particle, $\boldsymbol{v}(\boldsymbol{x},\tau)$ is the surface velocity field at that location and $\Delta \boldsymbol{X}_b(t)$ is the change in particle position due to its prescribed 'behaviour', expressed in a kernel. At each location the surface velocity field $\boldsymbol{v}(\boldsymbol{x},\tau)$ was obtained through linear interpolation of the ocean flow field data. In this work, to avoid particle beaching, a specific kernel was developed and used in all simulations to push back to their previous position those particles that had absolute velocity magnitudes below 0.001 m s^{-1}, which were only reached in proximity to land.

For the first par of this study, each simulation consisted in the backward advec-

Sampling location #	Latitude [°N]	Longitude [°E]	Date	Sampling location #	Latitude [°N]	Longitude [°E]	Date
1	-33.66477	18.03866	04/01/2019	13	-30.41112	-7.26208	12/01/2019
2	-33.51575	15.40349	05/01/2019	14	-29.99130	-11.58838	13/01/2019
3	-33.43135	13.62885	05/01/2019	15	-29.87998	-11.00460	14/01/2019
4	-33.31850	11.47783	06/01/2019	16	-29.87234	-7.99645	15/01/2019
5	-32.67499	7.03407	07/01/2019	17	-29.96830	-6.47338	15/01/2019
6	-32.55659	6.37040	08/01/2019	18	-29.98479	-3.94384	16/01/2019
7	-32.16113	3.61088	09/01/2019	19	-30.52156	-0.73241	18/01/2019
8	-31.84218	1.75581	09/01/2019	20	-30.83991	0.87086	18/01/2019
9	-31.53942	-0.32359	10/01/2019	21	-31.26654	2.81060	19/01/2019
10	-31.29263	-1.77394	10/01/2019	22	-32.16496	6.26655	20/01/2019
11	-30.92371	-3.59027	11/01/2019	23	-32.53798	9.33704	21/01/2019
12	-30.74764	-5.32828	11/01/2019	24	-32.99624	12.48462	22/01/2019

Table 2.1: Coordinates where and date on which microplastic sampling was undertaken during the NIOZ 2019 ‘South Atlantic Subtropical Gyre Plastics Cruise’.

tion of 24000 virtual particles (1000 per NIOZ 2019 sampling location, with random seeding within a 25 km^2 area centered at the sampling location) using the foruth-order Runge-Kutta method (RK4). The location of the particles was stored daily. The spatial domain of the analysis extended between latitude 0 - 70°S and longitude 73°W - 25°E. As soon as a particle left this domain during its advection, it was deleted from the simulation. Simulations lasted 5 model years (260 weeks) based on the findings of Wichmann et al. (2019), who argued that the maximum mixing time of the South Atlantic is 6 years and after that the information on the particle’s initial location is lost. Therefore, advecting particles backward for a longer period than the mixing time would produce meaningless results due to processes like the amplification of numerical error and the effects of varying integration schemes in a chaotic system such as the ocean surface.

Ocean flow fields

The eddy-resolving surface circulation ocean flow fields used here included a forecast and a reanalysis product, both obtained from the Copernicus Marine Environment Monitoring Service (CMEMS). The need to use two different products was determined by the fact that the Global Ocean Physics Reanalysis 1/12° (GLORYS12V1) product was available up until 26/12/2017, therefore not reaching the sampling time of the NIOZ expedition in 2019. On the other hand, the Global Ocean 1/12° Physics Analysis and Forecast Updated Daily only covered the time span between 01/01/2016 and Present, therefore not allowing for a five-year backward simulation. Both products use NEMO 3.1 ocean model (Madec and the NEMO team, 2008) and atmospheric forcing from ECMWF (European Centre for Medium-Range Weather Forecasts), but the Forecast product is based on a 3-hourly atmospheric forcing, while the Reanalysis one is based both on a 3-hourly and 24-hourly atmospheric forcing from ERA-Interim. As the two products overlapped for almost two years,

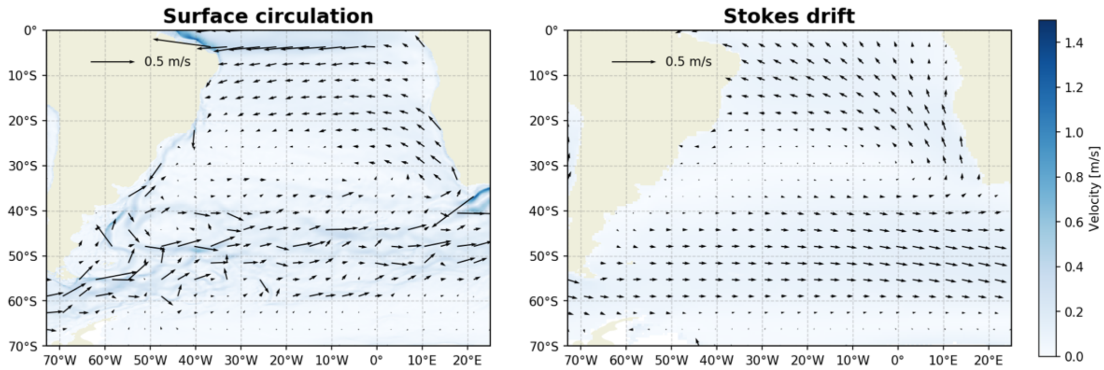

Figure 2.2: Average velocities between 01-01-2010 and 01-03-2019. The average velocities for surface circulation were calculated using the *SwitchDec2017* ocean flow field. The arrows indicate the direction and the colormap the magnitude of the velocity.

between 01/01/2016 and 26/12/2017, two ocean flow fields were created: one using the Reanalysis product from 2014 until 26/12/2017 and the Forecast product from 27/12/2017 until Present, named *SwitchDec2017*; and the other using the Reanalysis product from 2014 until 31/12/2015 and the Forecast product from 01/01/2016 until Present, named *SwitchJan2016*.

Before performing any analysis of virtual particle simulations, a comparison had to be made between the ocean flow fields used when advecting the particle backwards. Three simulations with particles seeded at the exact same locations were performed: one using the *SwitchDec2017* ocean flow field; a second one using the *SwitchDec2017* ocean flow field, but releasing particles seven days after their locations were originally sampled (therefore identified as *SwitchDec2017_deferred*); and the last one using *SwitchJan2016*. The three simulations ran for 5 years with an integration time step of 2 hours, recording particle location every day and tracking 24000 particles (1000 per NIOZ 2019 sampling location, with random seeding around the location).

Additional simulations were run including surface Stokes drift to the total ocean flow field. As Röhrs et al. (2012) and Fraser et al. (2018) argued that waves significantly affected the trajectories of surface drifters, it is hypothesised that the pathways followed by virtual particles in the simulations with Stokes drift differ substantially from those of particles advected in the general circulation flow field only. Zonal and meridional components of Stokes drift at the sea surface were obtained from the ECMWF ERA5 hourly product with a 0.5°x0.5° resolution. For computational ease, only the daily value at timestamp 00:00 was implemented in the simulation. This is consistent with the temporal resolution of the general circulation ocean flow field, which has a 24-hour resolution with timestamp set at 00:00.

The average velocities for surface circulation and Stokes drift over the domain can be seen in Figure 2.2.

Integration time step

The consistency between backward and forward simulations was assessed by comparing the trajectories of particles advected in an ocean flow field only consisting of the general circulation horizontal velocities. In order to do so, all the particles that remained in the South Atlantic basin for the entire backward simulation using the *SwitchDec2017* flow field were advected forward for 5 years from the date and location of their last observation in the backward simulation. Corresponding backward and forward simulations were run with integration time steps of 2 hours, 1 hour, 30 minutes and 15 minutes. At the end of the forward simulation, the distance d between the location where the particle was released in the backward simulation and the location where it was observed at the end of the forward simulation was calculated using the Haversine formula:

$$d = 2r \arcsin\left(\sqrt{\sin^2\left(\frac{\phi_2 - \phi_1}{2}\right) + \cos(\phi_1)\cos(\phi_2)\sin^2\left(\frac{\lambda_2 - \lambda_1}{2}\right)}\right) \tag{2.2}$$

where r is the average radius of the Earth with a value of 6371 km, ϕ_1 and ϕ_2 are the latitudes, and λ_1 and λ_2 are the longitudes of the two points.

2.3. Results

2.3.1. Ocean flow fields

The trajectories of virtual particles advected in flow fields with different characteristics were analysed by dividing the ocean domain into 1°x1° bins and calculating the probability that each bin was occupied by a particle during the entire simulation. As particle trajectories are deterministic, meaning that the same flow returns the same results, the differences observed in simulations performed with different ocean flow fields could only be due to contrasting flow conditions.

Both the simulations ran using the *SwitchDec2017* and *SwitchJan2016* flow fields showed a higher-probability area between latitude 25°S - 40° and longitude 15°W - 15°E (Figure 2.3A Top). Particles advected in the *SwitchJan2016* flow field had trajectories heading towards the northern part of the ocean basin and also transited more along the coastal areas compared to those advected in the *SwitchDec2017* flow field (Figure 2.3A Bottom). On the other hand, particles advected in the *SwitchDec2017* flow field had more trajectories visiting the south-westernmost part of the basin. Bins in the mid-latitudes showed a higher probability to be occupied by a particle during the entire simulation when particles were advected in *SwitchDec2017* rather than in *SwitchJan2016*.

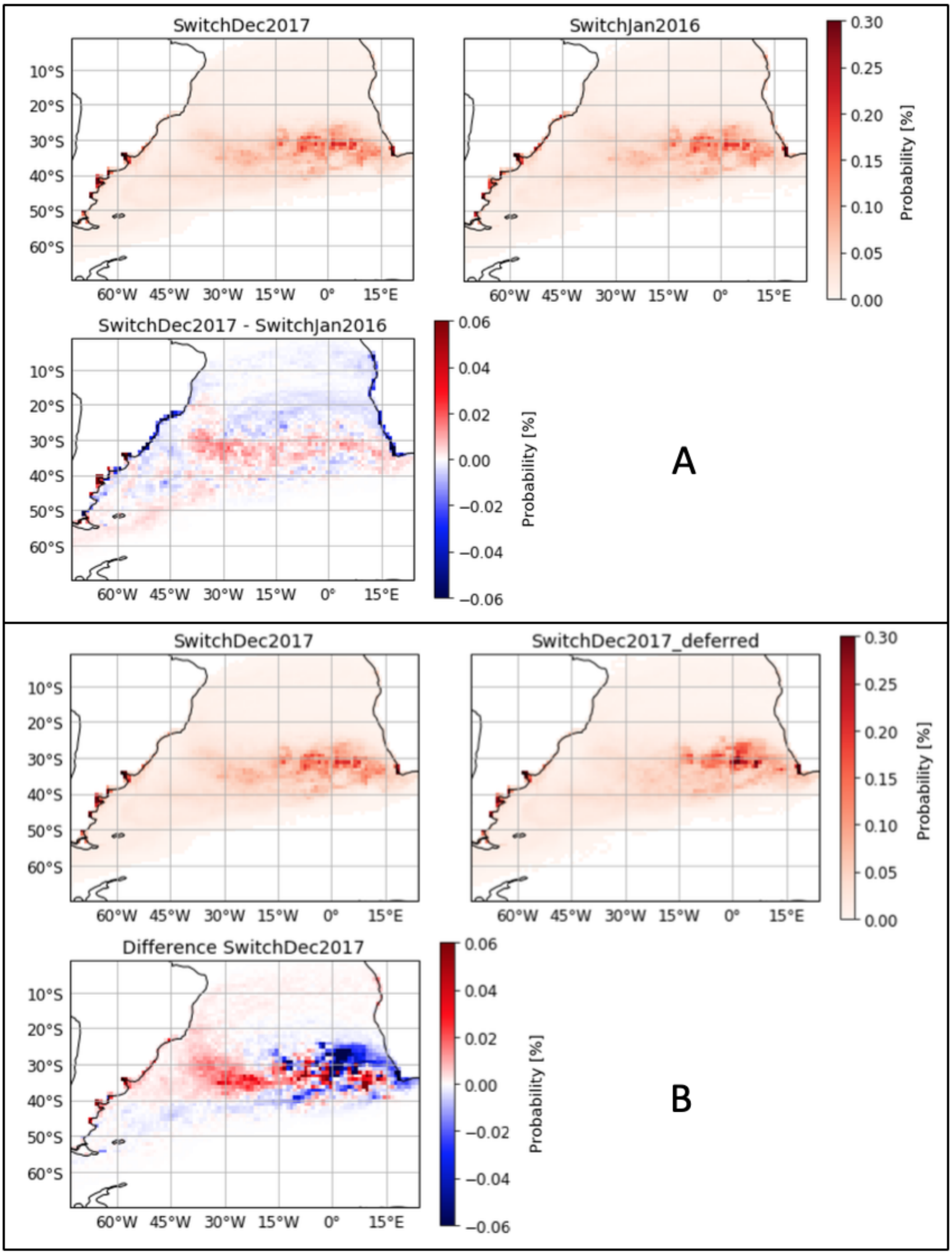

Figure 2.3: A) Top: Probability for *SwitchDec2017* and *SwitchJan2016* that a 1°x1° bin was occupied by a particle during the 5-year simulation. The sum of all the probabilities in the domain is 100. Bottom: Difference in probability values for each 1°x1° bin between the simulations ran using *SwitchDec2017* and *SwitchJan2016*. B) Top: Probability for *SwitchDec2017* and *SwitchDec2017_deferred* that a 1°x1° bin was occupied by a particle during the 5-year simulation. The sum of all the probabilities in the domain is 100. Bottom: Difference in probability values for each 1°x1° bin between the simulations ran using *SwitchDec2017* and *SwitchDec2017_deferred*.

Particles advected in the *SwitchDec2017_deferred* flow field also showed a higher-probability area in correspondence with that observed for *SwitchDec2017* and *SwitchJan2016*, even if the shape was slightly different. Moreover, some of the bins in that area in *SwitchDec2017_deferred* showed a much higher probability than in *SwitchDec2017* (Figure 2.3B Top). When looking at the difference between the values calculated from *SwitchDec2017* and *SwitchDec2017_deferred*, a rather distinct separation between the particle trajectories in the two ocean flow fields became visible (Figure 2.3B Bottom). When virtual particles were released on the same day as they were observed during the NIOZ 2019 expedition, their trajectories covered the north and western parts of the basin more than when they were released one week later. In this latter case, more particles occupied the bins off the coast of South Africa, dominating over the values observed for *SwitchDec2017* especially in the domain between 25 - 30°S and 0 - 15°E.

When particles were advected in an ocean flow field consisting of the sum of *SwitchDec2017* and surface Stokes drift (from here on *SwitchDec2017_wStokes*), their trajectories varied substantially from when they were advected in *SwitchDec2017* only (Figure 2.4). Bins in the area off the coast of South America had a much higher probability to be occupied by a particle during the *SwitchDec2017_wStokes* simulation than during *SwitchDec2017*. In agreement with this, bins in the area off the

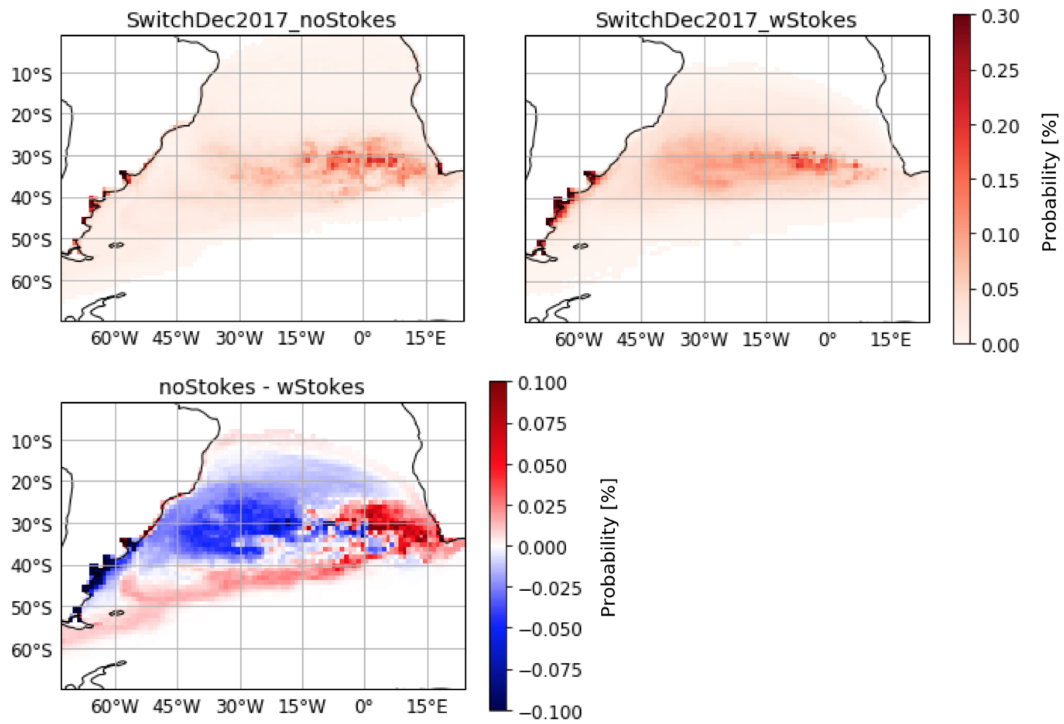

Figure 2.4: Top: Probability for *SwitchDec2017* without and with surface Stokes drift that a 1°x1° bin is occupied by a particle during the five-year simulation. The sum of all the probabilities in the domain is 100. Bottom: Difference in probability values for each 1°x1° bin between the simulations run using *SwitchDec2017* without and with surface Stokes drift.

coast of South Africa had a much higher probability to be occupied by a particle during the *SwitchDec2017* simulation.

2.3.2. Integration time step

Corresponding backward and forward simulations were run for 5 years and performed for ∼420 particles advected in *SwitchDec2017* with integration time steps of 2 hours, 1 hour, 30 minutes and 15 minutes. The exact number of particle differed slightly based on the integration time step considered, as more or less particles remained in the domain for the entire 5-year backward simulation (Figure 2.5).

Decreasing the time step from 2 hours to 1 hour produced a great improvement in the mean Haversine distance between the starting point of the backward and the ending point of the forward simulation, but the subsequent decrease from 1 hour to 30 and 15 minutes did not result in any further improvement. Additionally, the standard deviation values obtained for the four cases showed that the smallest mean Haversine distance was accompanied by the largest standard deviation (Table 2.2). The distributions of Haversine distances between the initial and final positions of corresponding particles released in backward and forward simulations obtained using different integration time steps were assessed by performing a Kolmogorov-Smirnov (K-S) test. Table 2.3 shows that the distributions were significantly different from each other, highlighting that the results obtained were dependent on the integration

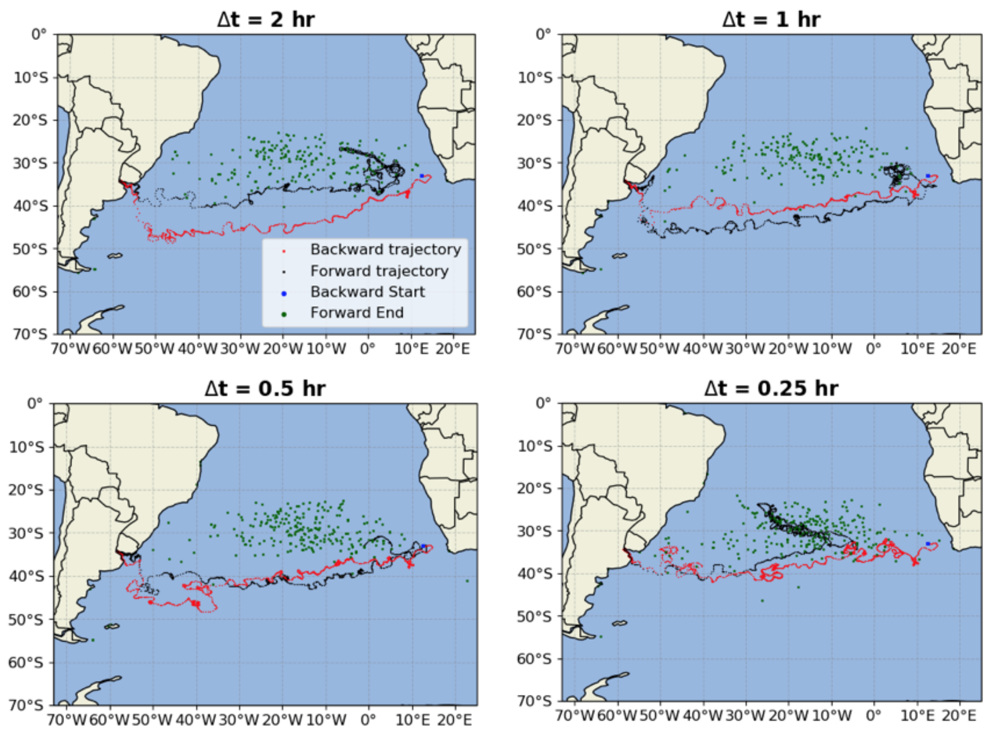

Figure 2.5: Example of the same trajectory calculated backward and forward with different integration time steps (Δt).

time step used.

For the backward and forward simulations ran with an integration time step of 1 hour the distance between corresponding particles was calculated for each point along their trajectories for the entire simulation (Figure 2.6). The separation distance was used to obtain the relative dispersion between the two particles over time, which was calculated as the square of the separation distance and is a measure of the spread of the particles around their centre of mass by the flow. Some particles separated early in their trajectory, and acted more as outliers as highlighted by the mean value of dispersion compared to the median. The latter showed that corresponding particles followed the same trajectory for about 200 days and then started separating, with their dispersion increasing quickly over time and reaching separation distances of hundreds of kilometres. The decomposition of dispersion in its meridional and zonal component revealed that a strong anisotropy started developing after about 10 days of simulation, with the zonal dispersion becoming one order of magnitude larger than the meridional. This result was not surprising, considering that particles were predominantly subjected to the eastward flow of the southern portion of the South Atlantic Subtropical Gyre.

2.4. Discussion

The results presented in the previous section showed how influential the ocean flow field and the integration time step were in determining the path followed by virtual particle in Parcels due to the chaotic nature of ocean flow (Wichmann et al., 2019).

The differences in probability with which each bin was occupied by a particle during course of the entire simulation resulted to be more significant when comparing particles advected in the same flow field but released a week apart (*SwitchDec2017* and *SwitchDec2017_deferred*; Figure 2.3B) than when advecting particles in two partially different flow fields (*SwitchDec2017* and *SwitchJan2016*; Figure 2.3A). This suggested that the internal variability of the system over a time period as short as one week was able to affect the trajectories of particles released more than when the flow field was partially different. The variability observed for a period of time as short as one week could be linked to the fact that particles were released in

Integration time step [h]	**2**	**1**	**0.5**	**0.25**
Mean [km]	2428	1820	2214	2507
Std [km]	1089	1464	1180	1251

Table 2.2: Mean and standard deviation of the Haversine distance between the ending location of the forward simulation and starting location of the backward simulation for corresponding particle trajectories calculated with different integration time steps.

one of the regions with the largest eddy kinetic energy in the world's oceans, where the the leakage of water from the Indian Ocean carried by the Agulhas Current produces the so-called Agulhas Rings (Rae, 1991). Therefore, the two combinations of CMEMS ocean field products proved to be consistent regardless of whether the switch from Forecast to Renalysis product took place in December 2017 or January 2016. It was decided to perform the switch in December 2017 so that the Reanalysis product would cover the majority of the simulation and also because Reanalysis was updated in light of observations while Forecast was not (Parker, 2016).

As hypothesised, the inclusion of surface Stokes drift into the ocean flow field in which the particles were advected highly affected their trajectories, with a higher probability of bins in the western part of the basin being occupied by a particle during the simulation. This is in agreement with Clarke and Van Gorder (2018) findings that Stokes drift is driven by the local wind condition and is in the direction of the wind. The main feature of atmospheric circulation in the South Atlantic is the South Atlantic Subtropical Anticyclone (or Subtropical High), which is semi-permanent and spreads between 15° - 45°S and 45°W - 15°E (Reboita et al., 2019). The anticyclonic circulation in the Southern Hemisphere is in anticlockwise direction, therefore explaining the differences observed between the trajectories of particles advected in *SwitchDec2017_noStokes* and *SwitchDec2017_wStokes* ocean flow fields. Below the Subtropical High, the Westerlies blowing over the South Atlantic increase transport due to Stokes drift from South America towards the east. This explains why the bins closer to the coast of South America had a much higher probability of being occupied by a particle in a backward simulation. Not all particles that were advected backwards reached the coastal area south of 35°S. Hence, the effect of Stokes drift on those particles that kept on being advected in the open ocean was to enhance their pathways northward towards lower latitudes off the coast of South America and then to push them towards more southern latitudes as a result of the action of Trade winds, explaining why bins at latitudes north of 30°S had a higher probability of being occupied by a particle when surface Stokes drift was added to the ocean flow field.

	0.25 hr	**0.5 hr**	**1 hr**	**2 hr**
0.25 hr	1	5.60E-26	2.00E-40	1.00E-16
0.5 hr	5.60E-26	1	4.80E-42	3.50E-24
1 hr	2.00E-40	4.80E-42	1	1.90E-39
2 hr	1.00E-16	3.50E-24	1.90E-39	1

Table 2.3: Difference in distance distributions obtained for the four integration time steps assessed. The table reports the *p*-values associated with the null hypothesis that two independent samples of distances were drawn from the same continuous distribution. Histograms of the distributions are available in Figure A.1.

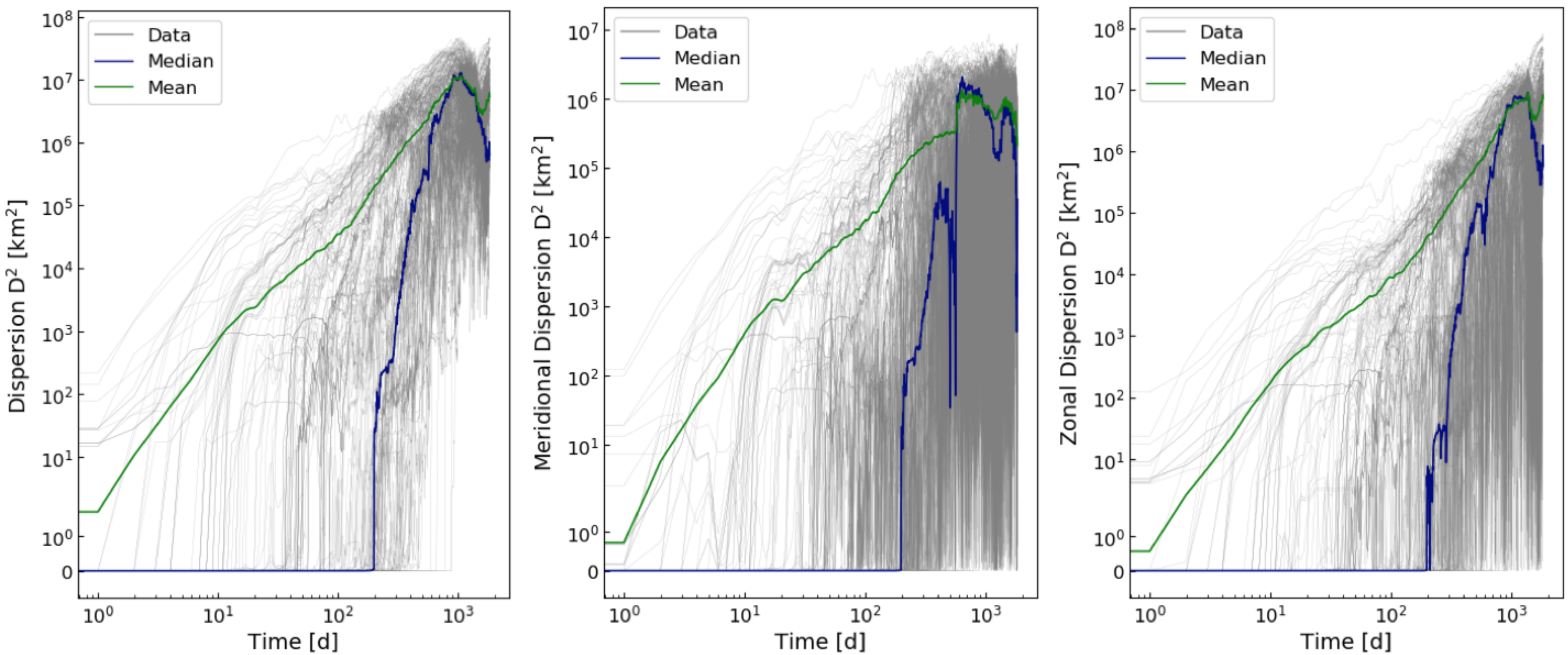

Figure 2.6: Total, meridional and zonal dispersion calculated for each pair of particles belonging to corresponding backward and forward simulations with an integration time step of 1 hour. Please note the different y-axis limit in the meridional dispersion plot.

The consistency between backward and forward simulations, which is a crucial element in the interpretation of results obtained from Lagrangian models, proved to be complicated. The difference in the trajectories and ending point of forward simulations versus the starting point of backward simulations was a direct consequence of how the position of a particle was calculated from equation 2.1. The position $\boldsymbol{X}(t + \Delta t)$ was obtained integrating the velocity $\boldsymbol{v}$ at position $\boldsymbol{X}(t)$ over the time step, but $\boldsymbol{X}(t)$ was different when going forward and backward, therefore different velocities were used for the integration. In light of this, it was expected that decreasing the integration time step would have returned an increased consistency between the trajectories of the forward and backward simulations, as reducing the interval of the integration would have decreased the distance travelled by the particle in the interval. However, it happened only when decreasing the integration time step from 2 to 1 hour. One explanation for this might be that the reduction of integration time step causes a larger propagation of the numerical error, as the position of the particle is evaluated more often than when the trajectory is computed using a larger time step.

Here, the comparison between backward and forward trajectories of individual particles was performed to obtain information on the reversibility of the second part of this study: the identification of sources of microplastic to the SASG. Therefore, investigating the exact mechanisms involved in the diversification of trajectories computed via backward and forward simulation lies outside of the scope of this project and future work is required to assess the differences of advecting particles in a Lagrangian framework backward and forward in time. Lagrangian simulation in backward mode remains a powerful tool to investigate the pathways of clusters of particles and their origin, which is the scope of the remainder of this study. Taking into account the results and considerations presented above, it was decided to proceed with this study advecting particles in an ocean flow field composed of both a horizontal general circulation component (*SwitchDec2017*) and surface Stokes drift and to use an integration time step of 1 hour. The trajectories of the particles released at the 24 sampling locations of the NIOZ 2019 cruise as a result of the 5-year simulation ran using these model settings are visible in Figure 2.7.

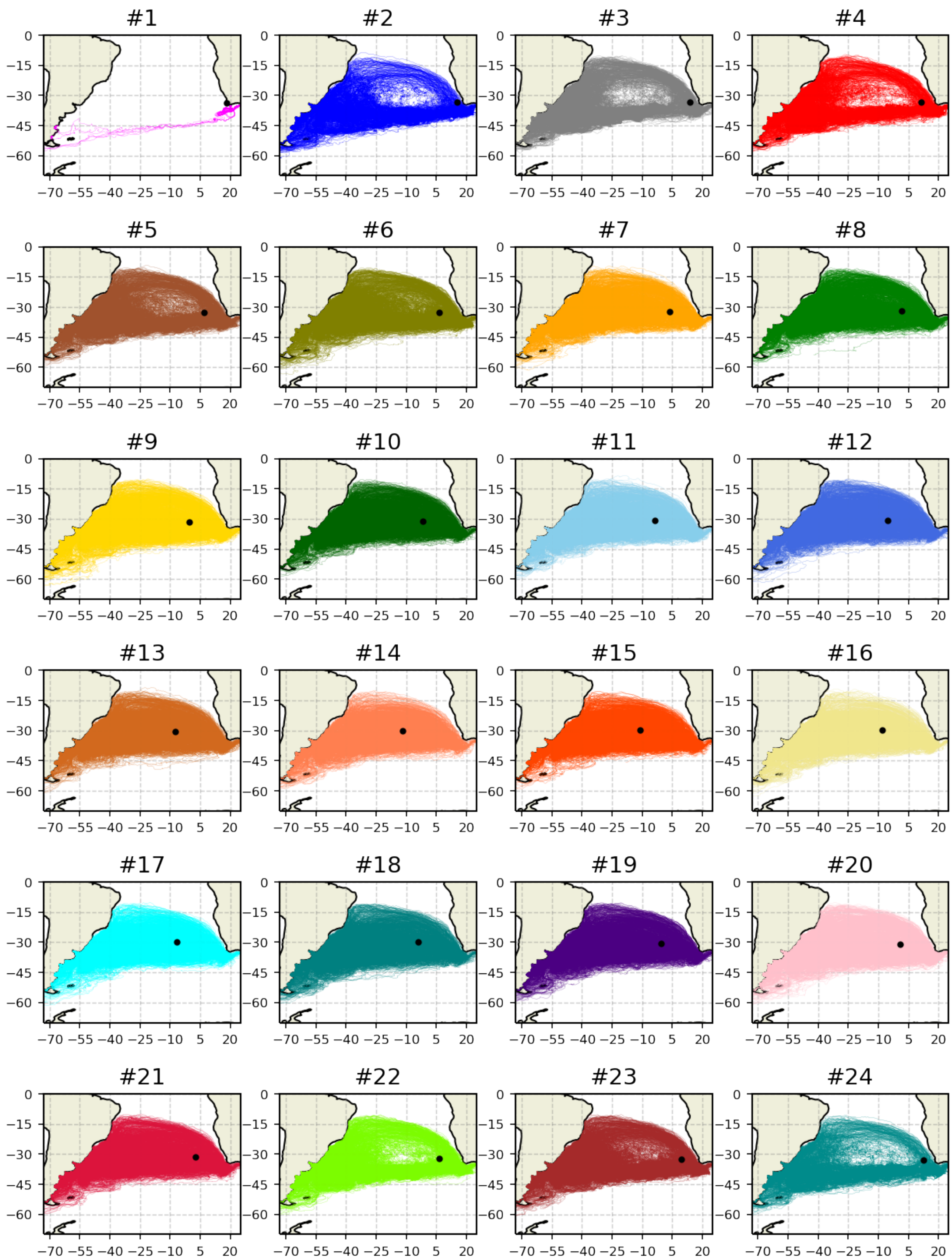

Figure 2.7: Trajectories of the 24 clusters of particles released at the NIOZ 2019 sampling locations, represented by the black dots.

3. Land sources of microplastics

3.1. Introduction

The advection of virtual particles backward in time allows not only to analyse the effects of ocean dynamics on the pathways followed by particles, but also to investigate where they originated. This is particularly important for microplastics, as identifying the most significant sources of pollution to the ocean could provide solid background information for the implementation of waste management policies on the national and international level. Microplastics are indeed often the product of the degradation of larger debris coming from land sources that mainly break down due to mechanical and chemical weathering (Andrady, 2011).

3.2. Methods

Based on population estimation data for 2019 (Demographia, 2019), the four most populous coastal cities on the eastern side and the five most populous on the western side of the South Atlantic basin were selected to assess their probability as land sources of microplastics (Table 3.1). An algorithm was developed that calculated the probability of each city being the source of each microplastic particle based on the trajectory it followed during the entire simulation. While here it was decided to investigate the probabilities of the most populous cities bordering the South Atlantic Ocean, the algorithm is not basin-specific and could be used to calculate the probabilities of other locations to be sources of microplastics in any backward Lagrangian simulation.

For this part of the study both the NIOZ 2019 sampling data and those retrieved from van Sebille et al. (2015) were used. In accordance with the results presented in Chapter 2, particles released at times and locations corresponding to the NIOZ 2019 sampling stations were advected in the *SwitchDec2017_wStokes* ocean flow field (this simulation will be referred to as *NIOZ 2019* from now on), while for those released at times and locations from van Sebille et al. (2015) the horizontal general circulation component of the flow field was obtained from CMEMS Global Ocean Physics Reanalysis 1/12° (GLORYS12V1) as it covered the entire time span

City	Country	Latitude [°N]	Longitude [°E]	Population [M]
Luanda	Angola	-8.82	13.22	7.645
Benguela	Angola	-12.58	13.39	0.565
Cape Town	South Africa	-33.93	18.56	4.260
Pointe Noire	Congo	-4.80	11.84	1.090
Rio de Janeiro	Brazil	-23.00	-43.30	12.070
Salvador	Brazil	-13.00	-38.45	3.325
Recife	Brazil	-8.09	-34.88	3.570
Buenos Aires	Argentina	-34.58	-58.36	15.130
Montevideo	Uruguay	-34.91	-56.15	1.325

Table 3.1: Cities selected as land sources of microplastics based on their population (Demographia, 2019) and location around the South Atlantic Ocean.

of the simulation, and Stokes drift was added to it (this simulation will be referred to as *van Sebille et al. (2015)* from here on). In order to have similar amounts of particles advected in the two five-year simulations, 24000 particles were released in total for *NIOZ 2019* (1000 per sampling location) and 27600 for *van Sebille et al. (2015)* (200 per sampling location). The trajectories of the 24 clusters of particles released in *NIOZ 2019* can be observed in Figure 2.7. To evaluate the influence of the advection time on the probabilities calculated for each source, these were also calculated based only on the first half (2.5 years) of the standard simulation.

The algorithm was implemented as follows. First, the Haversine distance (eq. 2.2) to each city was calculated for each point on the trajectory of the particles. The probability of each city being the source of the particle at each point on the trajectory was calculated following both an exponential ($\widetilde{P}exp_{p,s}$) and quadratic distribution ($\widetilde{P}quad_{p,s}$) in order to identify the effects of the modelling choices on the results obtained. In both cases, only the city closest to the particle at that point on the trajectory could be its source and therefore have a probability larger than zero, while all other cities could only have a zero probability of being the source of the particle at that point on the trajectory (Figure 3.1). For the exponential distribution the probability was calculated as:

$$\widetilde{P}exp_{p,s}(\beta, d_{p,s}) = \begin{cases} e^{-\frac{1}{\beta}d_{p,s}}, & \text{if } d_{p,s} \leq d_{p,k} \ \forall \ k \\ 0, & \text{otherwise} \end{cases} \tag{3.1}$$

where β is the scale parameter of the exponential distribution, $d_{p,s}$ is the distance from point p on the trajectory to city s and $d_{p,k}$ are the distances to all other cities. Since the value of β could not be found in or derived from any study available in the literature, $\widetilde{P}exp_{p,s}$ was evaluated for seven different values of β between 2.5 and 250 km. From a physical point of view, β represents the radius of the imaginary circle defining the 'catchment area' of each source and it is referred to as source uncertainty distance. The decision of modelling a circular 'catchment area' was based on the fact

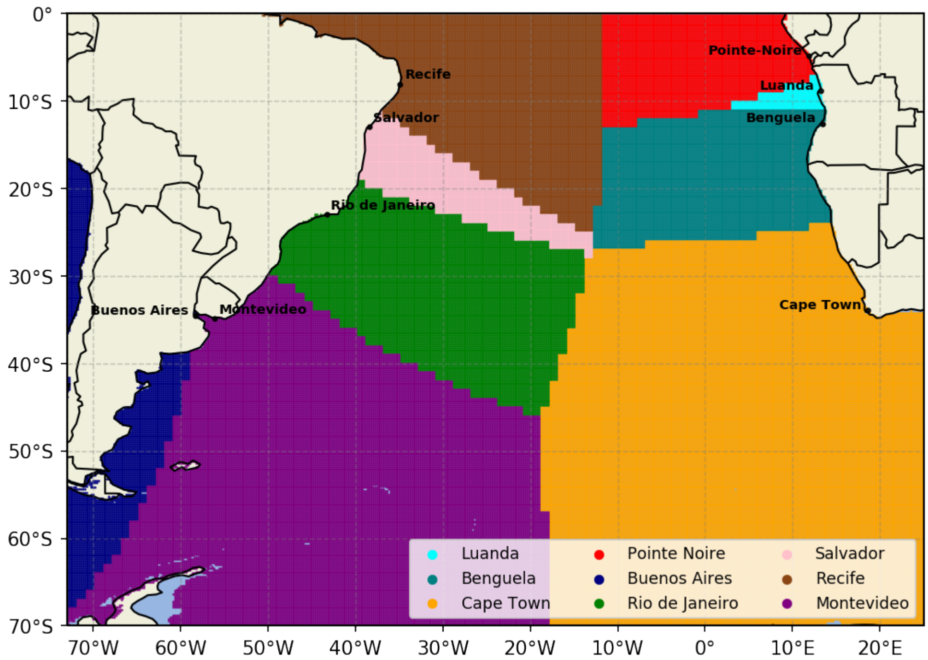

Figure 3.1: Subdivision of the South Atlantic Ocean into domains where only the closest city could be the source of the particle. Figure generated on a 0.2°x0.2° grid.

that a circular shape would better represent currents flowing in different directions, while using an elliptical 'catchment area' with a shorter radius towards the ocean and a larger one parallel to the coast would have caused longshore/boundary currents to affect more the probabilities obtained for the various land sources.

For the quadratic distribution the probability was calculated as:

$$\widetilde{P}quad_{p,s}(\beta, d_{p,s}) = \begin{cases} \left(1 - \frac{d_{p,s}}{3\beta}\right)^2, & \text{if } (d_{p,s} \leq 3\beta) \wedge (d_{p,s} \leq d_{p,k} \; \forall \; k) \\ 0, & \text{otherwise} \end{cases} \tag{3.2}$$

where β is the same source uncertainty distance used for the calculation of probabilities based on the exponential distribution and it is multiplied by a factor 3 in order for the two approaches to be consistent. In fact, one of the differences between the two implementations is that the calculation of probabilities based on the exponential law did not require to identify a cut-off distance after which the probability would be zero, as the exponential distribution tends asymptotically towards zero, while it was necessary to do so for the quadratic distribution. Based on the exponential distribution, a particle had a 5% probability $Pexp_{p,s}$ of being sourced from a given city when its distance to the source was:

$$\begin{aligned} 0.05 &= e^{-\beta d_{p,s}} \\ d_{p,s} &= -\beta ln(0.05) \\ d_{p,s} &\sim 3\beta \end{aligned} \tag{3.3}$$

Therefore, it was decided to use 3β as the cut-off distance after which a particle could only have a probability $\widetilde{P}quad_{p,s}$ equal to zero of being sourced from its closest city (Figure 3.2).

$\widetilde{P}exp_{p,s}$ and $\widetilde{P}quad_{p,s}$ depended only on the distance between the particle and the city evaluated, but did not take into account the time along the trajectory of the particle. In the real ocean, the effects of buoyancy and biofouling on microplastic were found to cause a decrease with time in the probability of a particle being still afloat on the surface of the ocean (Fazey and Ryan, 2016). Translated to backward modelling, this meant that it was more likely that a particle was sourced from the first city it was closest to during the simulation than at the following cities. Therefore, in order to include the history of the floating particle, the probabilities $\widetilde{P}exp_{p,s}$ and $\widetilde{P}quad_{p,s}$ were updated given that the particle was sourced from any city at previous points on the trajectory:

$$P_{p,s} = \begin{cases} \widetilde{P}_{p,s}, & \text{if } p = 0 \\ \widetilde{P}_{p,s} \cdot \left(1 - \sum_{l=0}^{p-1} \sum_{k} P_{l,k}\right), & \text{if } p > 0 \end{cases} \tag{3.4}$$

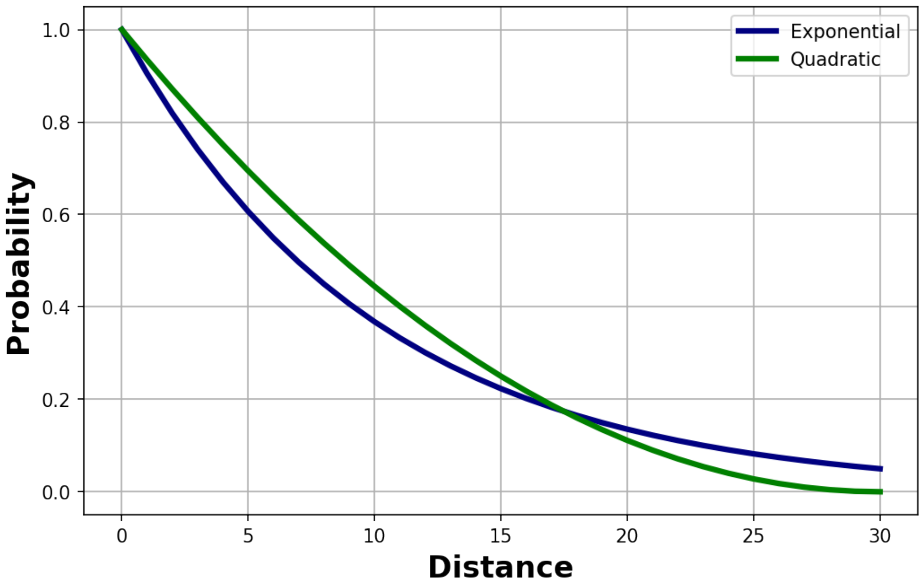

Figure 3.2: Exponential and quadratic decreases in probability with distance. Figure obtained with a source uncertainty distance (β) of 10.

where $\widetilde{P}_{p,s}$ represented both the exponential and quadratic implementation, as from this step onward the calculations were independent from the distribution chosen to calculate the probability based only on the distance. For each $p > 0$, the probability $\widetilde{P}_{p,s}$ was multiplied by the probability that the particle was not sourced from any city when evaluated at previous points along the trajectory.

Lastly, the overall probability with which a particle was sourced from city s was simply the sum of the probabilities with which it was sourced from that city when evaluated at all points p:

$$P_s = \sum_p P_{p,s} \tag{3.5}$$

The probabilities calculated for each individual particle were averaged over the number of particles advected in order to obtain the probability of each city as a source of microplastic to the South Atlantic Subtropical Gyre. In addition, the sets of 1000 particles released in the *NIOZ 2019* standard simulation were analysed individually to evaluate the sources of the microplastic samples collected at different locations during the expedition.

In order to assess the accuracy of the probability calculations, the bootstrap method (Efron, 1992) was used to estimate the mean and standard deviation of the probabilities that particles released in the South Atlantic Subtropical Gyre were sourced from the nine selected cities. Bootstrapping is a resampling technique based on the performance of inferential statistics on resampled data with sample size N that were independently sampled with replacement from existing sample data of size N. Sampling with replacement means that duplicates of values from the existing data sample are allowed in the bootstrap resamples. Here, 1000 bootstrap resamples were created and for each of them the probability of each city being the source of microplastic was calculated. From the distribution of the 1000 probabilities for each source it was possible to infer the mean value and how much it varied across all resamples.

3.3. Results

3.3.1. Sources of microplastics sampled during the NIOZ 2019 expedition

The analysis of the 24 individual particle clusters advected for 5 years in the *NIOZ 2019* standard simulation gave insight on how the release date and location influence the trajectories of the particles (Figures 2.7, 3.3 and 3.4). In addition, calculating the probabilities specifically for a given location rather than for the SASG as a whole system, could provide significant information for the biological assemblages that can be found on microplastic based on where it was retrieved and what path it followed to get there. Overall, the probabilities calculated for each of the 24 clusters showed much less variability when $\beta = 25$ km than when it was 100 km (Figures 3.3 and 3.4). From 1000 bootstrap resamples the mean and standard deviation of probability values for all sampling locations were calculated (Tables B.1 and B.2).

For $\beta = 25$ km, only sampling location #1 returned probabilties completely different with Cape Town dominating, while for all the other 23 locations the largest probability was that particles were sourced from somewhere else (Rest), represented by the black ring on the outside of the pie charts. The category Rest did not only include locations within the domain that were not considered as sources, but also the probability that particles were sourced from coastal areas bordering other basins. When considering only the known sources assessed, Montevideo was the most probable one, followed by Buenos Aires and Cape Town. Only location #2 had a probability of being sourced from Cape Town almost as large as in Montevideo. Rio de Janeiro and Salvador followed the other three cities in probability, and shared rather similar values overall. Probability values for each source at the 24 sampling locations can be found in Table B.1.

With a source uncertainty distance of 100 km, locations #1 and #2 returned an almost 100% probability of being sourced from Cape Town, and location #24 a probability slightly larger than 50% (Table B.2). For all other locations the most probable source was again Montevideo, but Cape Town and Rio de Janeiro also had significant values. In particular, Cape Town resulted to be a more probable source for particles coming from sampling location #3, #4, #6 and #23, while Rio de Janeiro for all the others, with values much larger than Cape Town for all sampling points located westward of 5°E.

The values obtained for location #1 represented clear outliers both when probabilities were obtained with β equal to 25 and 100 km, and they were the most consistent between the two calculations. As a matter of fact, sampling location #1 was $\sim$ 20 km from the coast north of the Cape and the majority of the particles released there remained in the area for the entire simulation because of the unresolved morphology of the Cape Town area or left the domain to the Indian Ocean (Figure 2.7). Contrarily, microplastics released at sampling point #2 had the largest probability of being sourced from Montevideo when β was 25 km, but had an almost 100% probability of coming from Cape Town when β was 100 km. An analogous result could be observed for sampling location #24, for which Cape Town dominated when probabilities were calculated with a source uncertainty distance of 100 km and Montevideo of 25 km. In particular, sampling location #2 was less then 300 km from Cape Town, which meant that with $\beta = 100$ km, the probability of the particles released there of being sourced from Cape Town just based on the release location was already larger than 5%.

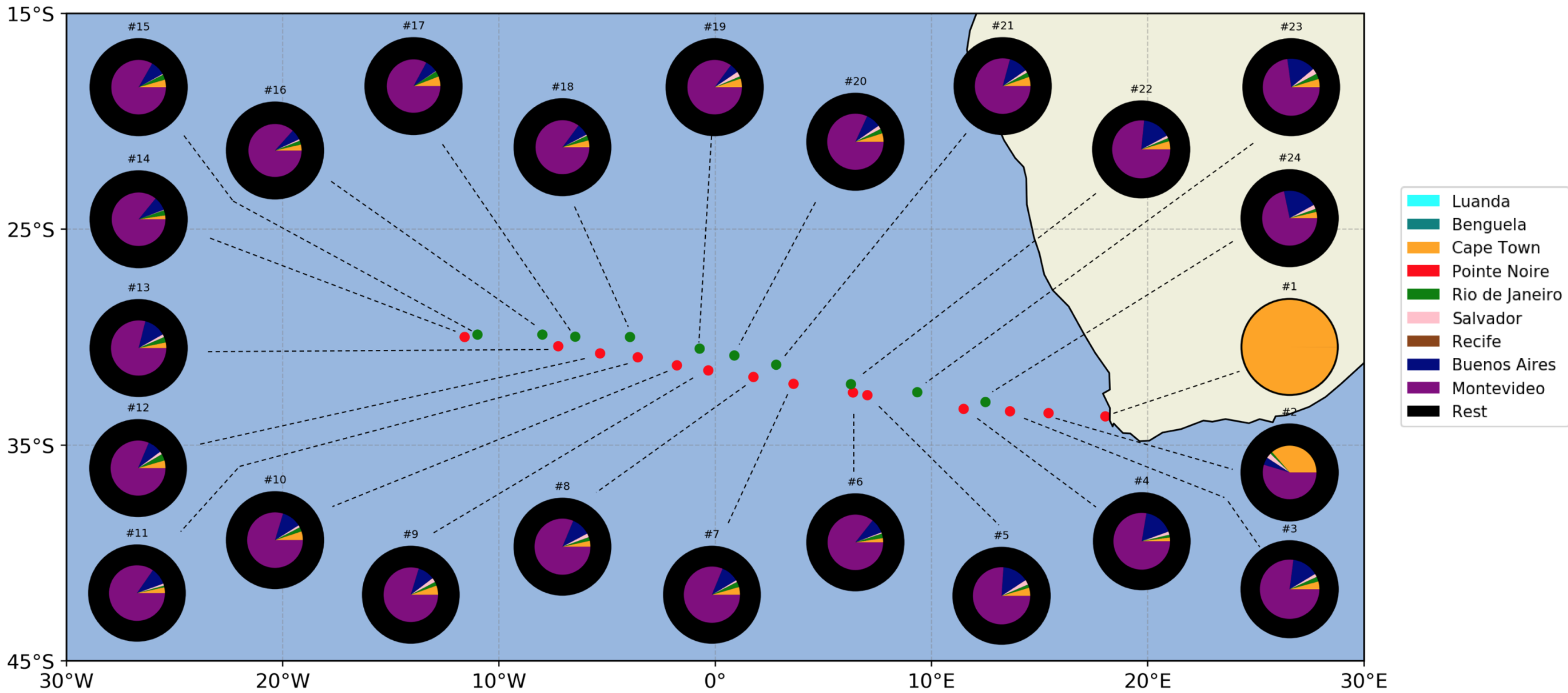

Figure 3.3: Probabilities calculated with $\beta = 25$ km with which microplastic samples retrieved at each of the NIOZ 2019 sampling locations were sourced from each of the nine selected cities and from somewhere else (Rest). The thickness of the black ring represents the probability of particles not being sourced at the nine cities (Rest). Values are listed in Table B.1.

While it was the second most probable known source when β was 25 km, Buenos Aires' probability was relevant only for sampling locations #3 –#5 and #22 –#24 when β was 100 km. The opposite could be observed for Rio de Janeiro, which stood out as the second most probable source for the majority of NIOZ 2019 sampling locations when β was 100 km, but was almost irrelevant for all of them when β was 25 km.

The outward-bound leg of the journey reached sampling location #14 as its north-westernmost point (Table 2.1), after which the expedition headed back to Cape Town. The two closest sampling locations were #6 and #22, which were at a distance of 44 km, followed by locations #14 and #15 which were 57 km apart. Particles released at location #6 and #22 showed more significant discrepancies in their source probabilities than those released at #14 and #15 for both values of source uncertainty distance. An explanation could be found in the internal variability of the system and follows on the results presented in Section 2.3, as the two sampling points were visited 12 days apart during the cruise and so were the particles released during the simulation (Table 2.1).

3.3.2. Sources of microplastics to the Gyre

In regard to the probabilities of each of the nine cities to be the sources of microplastics to the SASG, in all cases considered the mean values calculated from the 1000 bootstrap resamples converged to the probabilities obtained for the four original samples (two each for the *NIOZ 2019* and *van Sebille et al. (2015)* datasets, one considering the entire 5 years of simulation and the other considering only the first 2.5 years). Therefore, the results presented here show the means and standard deviations derived from inferential statistics performed on the bootstrap resamples. All probability values can be found in Tables B.3 - B.10. As the size of bootstrap resamples was large and the standard deviation values obtained were low, it could be argued that the mean probability values are a precise representation of the population. In general, larger probability values also had larger standard deviations, but the coefficient of variation (the ratio between the standard deviation and the mean) increased as probability values decreased. This suggested that the estimates of source probabilities were more accurate for sources with a higher probability and it is in agreement with the fact the a change in the number of times sources with lower probabilities in the original samples were represented in the bootstrap resamples generated more variance than a change in the representation of probabilities that were already high in the original samples.

Figures 3.5 and 3.6 show that, as expected, an increase in source uncertainty distance (β) resulted in a general increase in probability of particles being sourced from the selected cities and consequently a decrease in the probability of being

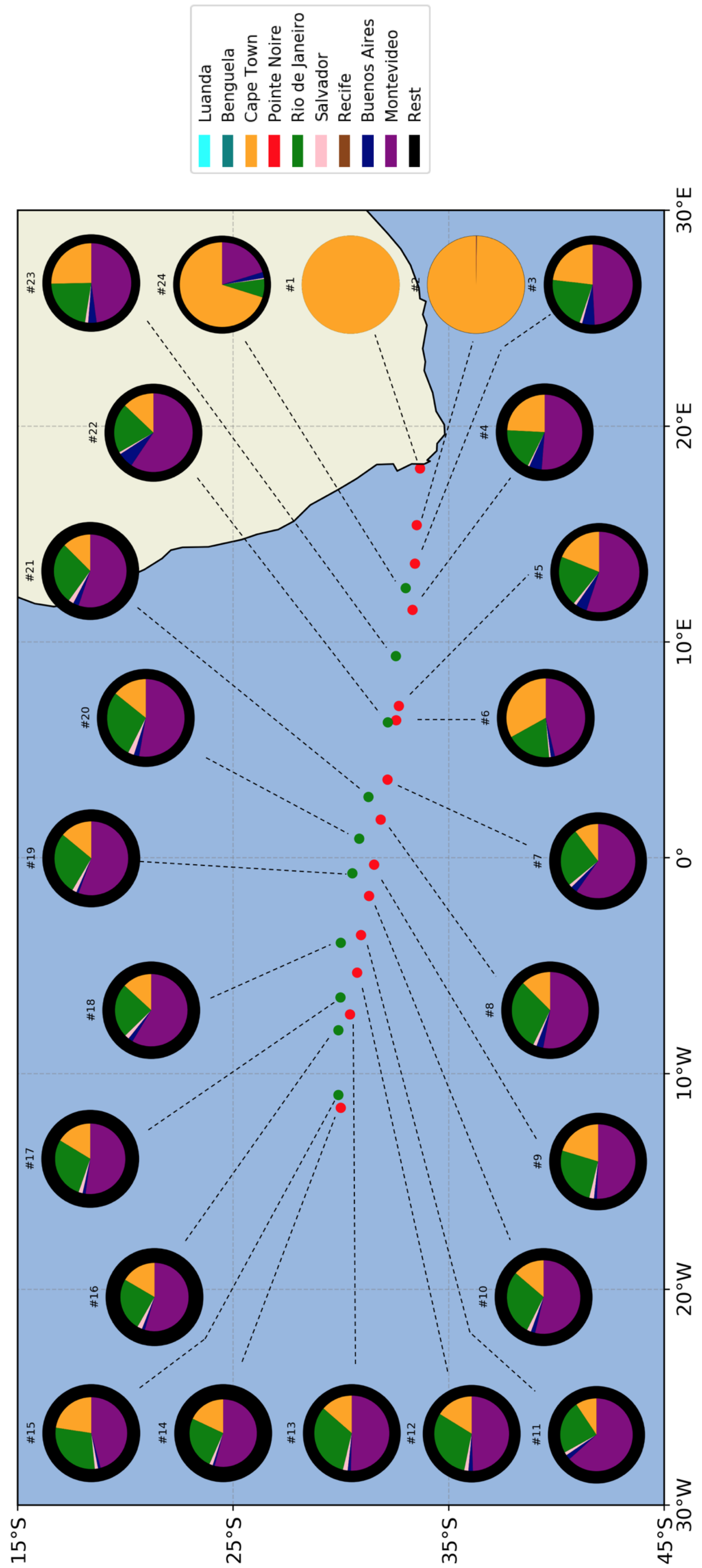

Figure 3.4: Probabilities calculated with $\beta = 100$ km with which microplastic samples retrieved at each of the NIOZ 2019 sampling locations were sourced from each of the nine selected cities and from somewhere else (Rest). The thickness of the black ring represents the probability of particles not being sourced at the nine cities (Rest). Values are listed in Table B.2.

sourced from somewhere else (Rest) both when calculated using the exponential and quadratic distribution. Probability values calculated with smaller values of β resulted to be more coherent among exponential and quadratic modelling, while diverging quite significantly for β values larger than 100 km, with the exponential distribution returning higher probabilities than the quadratic. Nevertheless, the order of sources based on their probability remained relatively consistent between corresponding exponential and quadratic results, besides for the largest value of β considered (250 km). Since the comparison is between models and not datasets, as the results are a function of the release locations, the two are presented in the following subsections separately. Nevertheless, many features that distinguished the exponential and quadratic approaches were observed in both *NIOZ 2019* and *van Sebille et al. (2015).*

NIOZ 2019

The two models returned Buenos Aires as the city with the highest probability when β was 1.43 and 10 km, followed by Montevideo and Cape Town, both when assessing the full 5 years and only the first 2.5 years of the trajectories (Figure 3.5). In the case of the 2.5-year trajectories, the standard deviation values obtained for Montevideo and Cape Town for β = 2.5 and 10 km were almost identical, not allowing to differentiate the two sources as one more likely than the other. When β increased to 14.3 km, Montevideo became the most probable source as calculated using the exponential model, but Buenos Aires remained the most probable when following the quadratic approach. Again, the two models gave back consistent results for *NIOZ 2019* when calculations were performed with $\beta = 25$ km.

For source uncertainty distances of 100 and 143 km, the standard deviations of Cape Town and Montevideo, the two most probable sources, gave rise to an overlapping interval between three standard deviations above and below the mean among the two sources when calculated following the quadratic approach, but this was not observed for the exponential when the entire 5-year trajectory was considered. For β values greater than 100 km, Buenos Aires' probability went down to zero for all cases assessed using the quadratic distribution, while it had slightly larger values when calculated with the exponential approach.

The largest values of β assessed was 250 km, which returned significant differences between the results obtained from the two models. As a matter of fact, the exponential approach produced a relative order of most to least probable source that was different than that obtained for $\beta = 143$ km and also different than that obtained following the quadratic distribution. When β was 143 km the three most probable land sources of microplastics were Montevideo, Cape Town and Rio de Janeiro. This did not change for $\beta = 250$ km using the quadratic distribution, but it became Cape Town, Rio de Janeiro and Montevideo when using the exponential model.

The probabilities calculated only considering the first 2.5 years of the trajectories were generally lower than the corresponding ones obtained from the 5-year trajectories. The values obtained from the exponential distribution were the most consistent between 5-year and 2.5-year calculations for $\beta = 250$ km, in particular for Cape Town.

van Sebille et al. (2015)

Buenos Aires resulted to be the most probable source when probabilities were calculated using the two smallest values of β following the exponential approach and the three smallest values following the quadratic approach (Figure 3.6). The city with the second-highest probability for source uncertainty distances of 2.5 and 10 km as obtained from the exponential model was Montevideo, which became the most probable source when β was increased to 14.3 km. Montevideo was also the second most probable source obtained for source uncertainty distances between 2.5 and 14.3 km when calculated following the quadratic distribution. The relative order of sources was inconsistent between the two models also when calculations were performed with $\beta = 25$ km, with Buenos Aires being the third most likely source when calculated with the exponential distribution but the second one with the quadratic distribution.

When source uncertainty distance was increased to 100 and 143 km, the probability values and the interval between three standard deviations above and below the mean overlapped completely for Cape Town and Montevideo both when using the exponential and quadratic distribution. Analogously to what observed in *NIOZ 2019*, for β values greater than 100 km Buenos Aires' probability reached zero for all cases assessed using the quadratic distribution, while the values calculated from the exponential distribution were marginally larger.

For $\beta = 250$ km, contrasting results were obtained from the two modelling approaches. In this case, the exponential distribution returned an order of most probable sources that differed from that obtained following the quadratic distribution and also the exponential distribution with $\beta = 143$ km, with Rio de Janeiro dominating over Cape Town and Montevideo. Rio de Janeiro's and Cape Town's intervals between three standard deviations above and below the mean slightly overlapped in the exponential modelling and Cape Town's and Montevideo's overlapped completely in the quadratic modelling results. Additionally, the exponential model returned probability values between 1 and 3% for Benguela, Salvador and Recife, while they were all lower than 1% when calculated following the quadratic distribution. As returned from the exponential approach, Luanda and Pointe Noire also had probability values

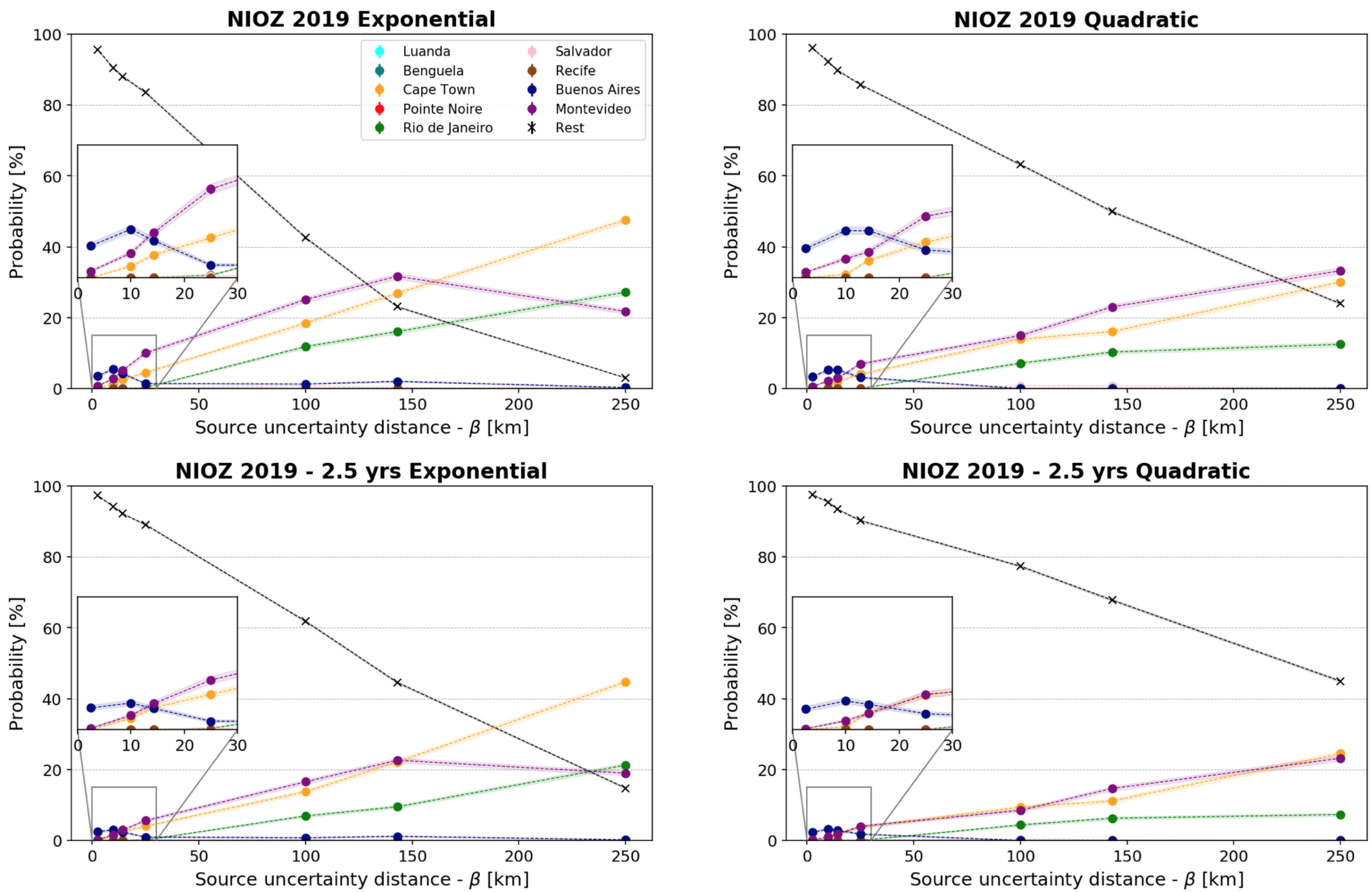

Figure 3.5: Source probabilities calculated for *NIOZ 2019* using the exponential and quadratic distribution when considering the entire trajectories of the particles (Top) and only the first 2.5 years (Bottom). The solid line represents the mean obtained from the 1000 bootstrap resamples and the shaded region the interval between three standard deviations above and below the mean.

slightly larger than zero. This was the only case in which the northernmost African cities considered for the study resulted as probable sources of microplastics to the South Atlantic Subtropical Gyre.

The differences between probabilities calculated only considering the first 2.5 years and the full 5 years of the trajectories were more remarked for low values of source uncertainty distance. The limited variability obtained for larger values of β could be attributed to the fact that release locations in this dataset were spread out over the entire basin.

3.4. Discussion

While simulations of microplastic dynamics by means of Lagrangian modelling forward in time have previously allowed to identify accumulation areas of debris in all ocean basins (van Sebille et al., 2015; Eriksen et al., 2014), to date no studies have been published on the potential of using backward trajectories to assess the sources of microplastic found in the ocean gyres. The methods developed for this study were used here to assess the relative contribution of different coastal cities to the pollution of the South Atlantic Ocean, but the same algorithm could be applied to any type of source and any basin once the trajectories of the particles are known.

The soundness of the methodology can be inferred from the consistency between the results obtained across all computations performed on the two datasets both following an exponential and quadratic distributions. For all source uncertainty distances considered excluding 250 km, the quadratic and exponential approaches returned very similar relative orders of cities from the most to least probable between corresponding cases and for the lowest values of β also coinciding values.

The choice of modelling the probability with which a particle was sourced from a given source based on its distance both following an exponential and quadratic distribution was arbitrary, and the two approaches produced different results due to their intrinsic characteristics. The exponential modelling returned a sharper decrease in probability with distance for smaller distances and did not require a limit to the 'catchment area' of each source, as the exponential distribution tends asymptotically towards zero. On the other hand, probabilities obtained from the quadratic modelling decreased more moderately with distance at the beginning of the distribution, but then showed a stronger decrease than those obtained from the exponential model as distance increased and they became zero for distances equal and larger than the cut-off radius (three times the source uncertainty distance, eq. 3.2). For the smallest two source uncertainty distances, the two approaches returned similar results but they progressively differed with an increase in β. For the largest β, the two modelling choices resulted in a significant discrepancy both in magnitude

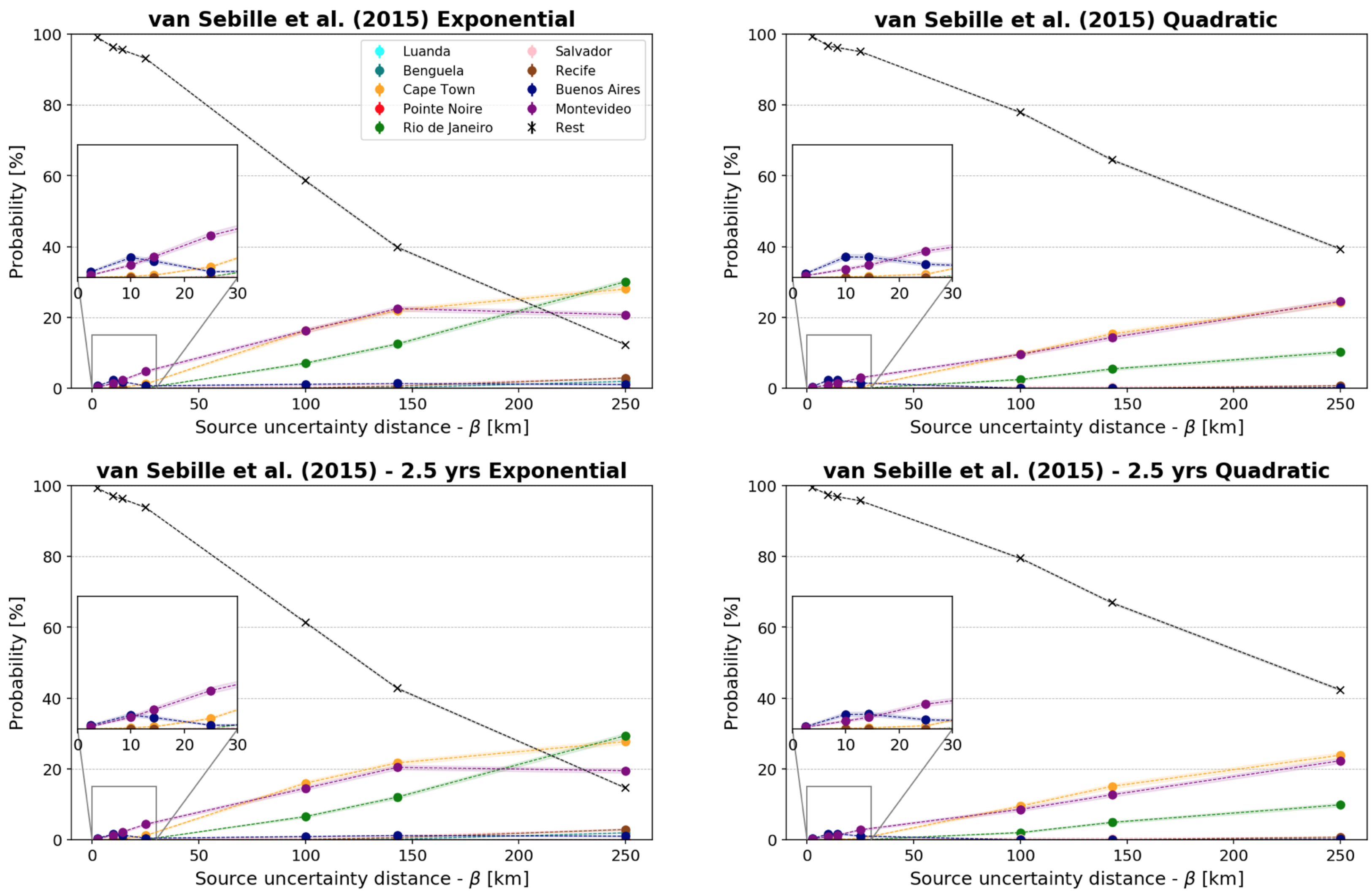

Figure 3.6: Source probabilities calculated for *van Sebille et al. (2015)* using the exponential and quadratic distribution when considering the entire trajectories of the particles (Top) and only the first 2.5 years (Bottom). The solid line represents the mean obtained from the 1000 bootstrap resamples and the shaded region the interval between three standard deviations above and below the mean.

and relative order of the most probable sources.

The coherence between the results observed in both simulations when particle trajectories were considered for 5 and 2.5 years suggests that for a value of β as large as 250 km, particles reached a 100% probability of being sourced at one or more of the selected cities in the earliest part of their trajectory. As a matter of fact, from the computation of $P_{p,s}$ followed that a particle only had a 5% probability of being sourced at a given city when the distance $d_{p,s}$ was larger than $-\beta\ln(0.05)$ (Eq. 3.3). For $\beta = 250$ km, that became $d_{p,s} > 749$ km, and from the distribution of the sampling locations observed in Figure 2.1 it can be seen that many sampling points were located within 750 km ($\sim 8°$ longitude at a latitude of 30°S) from the coast and source cities. Therefore, it is argued that the probabilities calculated through exponential modelling with $\beta = 250$ km are in many cases reflecting the locations where particles were released during the Lagrangian simulation. On the other hand, the more pronounced decrease in probability for larger distances and the cut-off radius of the quadratic distribution returned significantly smaller probabilities than those obtained from the exponential approach for β equal to 250 km. Hence, for large uncertainty distances the results obtained from quadratic modelling were less biased on the release location than those obtained from exponential modelling.

Assessing the probability of both Buenos Aires and Montevideo as sources of microplastics instead of having them together as a single source highlighted some of the strengths and limitations of the methodology. The two cities are located on the estuary of the Río de la Plata, with Montevideo being closer to the ocean than Buenos Aires. As the algorithm developed only allowed the closest city to the particle to be its source (eq. 3.1 and 3.2), Montevideo always prevailed over Buenos Aires unless the particles reached the most inland part estuary or when they were close to the continent at latitudes lower than the Río de la Plata estuary. The latter case resulted in an unrealistic division between the two cities, as the distance was calculated on the great circle and for Buenos Aires specifically did not reflect the morphological and oceanographic configuration of the real system. When they reached the estuary, the morphology and resolution of the data caused the particles to get stuck there for the remainder of the simulation and spend an important amount of time closer to Montevideo and Buenos Aires, which was unrealistic. The majority of particles that reached the estuary already had a 100% probability of being sourced from cities other than Buenos Aires when this was calculated using larger values of β, but this was not the case for β equal to 2.5, 10 and 14.3 km. Smaller source uncertainty distances favoured Buenos Aires over Montevideo as a source for the particles that reached the estuary because the coordinates of the former were closer to the ocean than those of the latter. For these reasons the probability of Buenos Aires as a source of plastic to the SASG increased with a decrease in β, while that of Montevideo simultaneously decreased. Therefore, the interpretation of Montevideo as a dominant source when probabilities were calculated with $\beta = 25$, 100 and 143 km is better revisited as the dominance of the Río de la Plata and its estuary as sources, especially if one considers the much larger population of Buenos Aires than of Montevideo.

In general, even if assessing probabilities with values of β as low as 2.5, 10 and even 14.3 km allowed to identify the underlying mechanisms behind the discrepancies in the results obtained for Montevideo and Buenos Aires, such low values of source uncertainty distance can hardly be supported from a geographical and physical point of view. Coastal cities of sizes such as those considered here are spread out for more than 10 km along the coast and representing them as one point located at arbitrary coordinates, even if accurately selected, did not account for the whole picture. In fact, in the case of Cape Town the morphology of the area lead to the choice of a location that was further inland than 2.5 km in order for it to be located not too far from one side of the Cape or the other. Additionally, the ocean flow fields obtained from CMEMS Reanalysis and Forecast products had a resolution of 1/12° ($\sim$ 9 km), while the ERA5 Stokes drift data had a resolution of 0.5° ($\sim$ 55 km) at the Equator (6.5 and 39 km respectively at latitude 45°N/S). In the case of $\beta = 2.5$ km, particles only have a probability smaller than 5% of being sourced from a given city when using the exponential and 0% when using the quadratic approach for distances $d_{p,s} >$ 7.49 km (eq. 3.3),which is less than the resolution of the highest-resolved product used for this study.

All the five cities closer to the Equator showed much lower probabilities of sourcing microplastics to the SASG, but in particular the three on the African coast (Benguela, Luanda and Pointe Noire) had a 0% probability for all the *NIOZ 2019* simulations, both using exponential and quadratic modelling, and only Benguela had a probability larger than 1% of being the source of microplastics to the SASG, when calculated with β equal to 250 km in *van Sebille et al. (2015)* using the exponential distribution. The trajectories in Figure 2.7 show how no particles were advected close to the three northernmost African cities in the *NIOZ 2019* standard simulation. This is consistent with Onink et al. (2019) finding that particles released at those locations and advected forward in time crossed the Equator and were located in the North Atlantic basin at the end of the 12-year simulation.

The South Atlantic Ocean is a highly-connected basin (Froyland et al., 2014; Onink et al., 2019; Wichmann et al., 2019) and a significant amount of particles advected in the simulations left the study domain both at 25°E to the Indian Ocean and at 75°W in correspondence of Drake's Passage. When a particle left the domain, it was given coordinates of 90°N 0°E for the remaining part of the simulation, so that it would be located at far enough distance not to have any probability to be sourced from one of the nine cities. Therefore, the category Rest does not only include locations within the domain that were not considered as sources, but also the probability that those particles were sourced from coastal areas bordering other basins. In particular, Onink et al. (2019) calculated that after 12 years of advection forward in time, almost 40% of the particles located in the South Atlantic were initially released in the Indian Ocean and 9% in the South Pacific. In the real ocean, however, particles would be able to re-enter the domain considered after leaving it, while this option was not taken into account in the simulations. Hence, the decision of deleting particles as soon as they left the domain might have caused a loss in information on source probabilities.

An important consideration on the procedure developed to calculate source probabilities is that it did not take into account the role played by the temporal resolution of the individual particle's trajectory. In this study, the position of each particle was saved once per day in the output of the Lagrangian simulation, hence the probabilities were obtained from the daily location of the particle. A change in the temporal resolution of the particle's trajectory would cause a change in the source probabilities obtained, as calculations would be based on more (less) points along the same trajectory if the output of the Lagrangian simulation were saved more (less) frequently than once per day. As particles could have a maximum cumulative probability of being sourced from the nine selected cities of 100%, probabilities assessed more often along the trajectories would likely cause particles to reach a cumulative 100% probability earlier in time than when probabilities are calculated based on less points on the trajectory, and vice versa. Therefore, as future work, the computation of source probabilities needs to be standardised in such a way that they would not be affected by the temporal resolution of Lagrangian simulations' outputs.

The implementation of the history of the particle as the update in probability given that the particle was sourced from somewhere in the earlier stages of the trajectory was a realistic approximation that could be improved with the availability of new data. Fazey and Ryan (2016) argued that it takes between 17 and 66 days for plastic debris of various sizes to reach a 50% probability of sinking due to biofouling, but their experiment was performed in harbour waters in a controlled setting and no open ocean data are available at the moment. In the real ocean buoyant microplastic particles are subjected to biofouling and therefore sink to the deeper layers and the bottom of the ocean once the growth of organisms makes them denser than seawater. Hence, the assumption that the first city to be passed-by by the particle in a backward simulation had a larger probability to be its source than the cities passed-by later reflects the likelihood that an increase in the time spent afloat would result in an increase of the probability of the particle not being on the surface of the ocean anymore. On the other hand, it is highly unlikely that a particle would stay afloat for five years (Koelmans et al., 2017), so implementing a decrease in time regardless of whether particles were sourced at previous points on the trajectory might return more accurate results.

4. Conclusion

Previous studies based on modelling microplastics dynamics forward in time within a Lagrangian framework allowed to identify the Subtropical Gyres of all oceans as accumulation areas of debris, but to date no previous work had identified the land sources of microplastics found in the Gyres using trajectories obtained from backward Lagrangian models. The study presented here analysed the trajectories of microplastics particles advected backward in time for 5 years in the South Atlantic Ocean. Particles were released at locations corresponding to the sampling points of the NIOZ 2019 ‘South Atlantic Subtropical Gyre Plastics Cruise’ and those retrieved from van Sebille et al. (2015) and were advected in an ocean flow field consisting of the sum of surface general circulation and Stokes drift. No single general circulation flow field was available for the five years between 2014 and 2019 when the simulation was run for particles representing those collected during the NIOZ 2019 cruise, thus a Reanalysis and a Forecast product from CMEMS had to be combined to obtain a flow field continuous in time. As the two products overlapped for almost two years, the trajectories of particles advected in two flow fields in which the switch from Reanalysis to Forecast product took place at different times between 2016 and 2017 were analysed and showed that there were no significant discrepancies between the Reanalysis and Forecast velocities. Additionally, Stokes drift has been proven to significantly affect the pathways followed by the particles. Lastly, the step-wise computation of particle trajectories was proven to return inconsistencies between corresponding backward and forward simulations.

Nine of the most populous coastal cities bordering the South Atlantic Ocean were chosen as land sources and their probability of sourcing plastics to the South Atlantic Subtropical Gyre was calculated based on the distance between the particle and the source at each point on the trajectory. Probabilities were calculated following both an exponential and a quadratic distribution in which the probability of a city being the source of the particle decreased with an increase in distance and was also a function of the parameter β, the source uncertainty distance, that reflected the radius of the ‘catchment area’ of each source. Moreover, the history of the particle was taken into account, making it more likely that particles were sourced at the city/cities to which they passed by in the earlier stages of their trajectories. A sensitivity analysis was performed using seven values of β varying between 2.5 and 250 km, which returned a significant increase in probability values for different sources with an increase in β, especially when calculated with the exponential distribution.

The probabilities calculated for the *NIOZ 2019* and *van Sebille et al. (2015)* simulations returned consistent values among the exponential and quadratic approaches especially for values of β between of 25 and 100 km. This was also the range identified as the most meaningful from a geographical and physical point of view, as it is able to capture the size of cities as large as those considered here. The sources that returned the highest probabilities were the Río de la Plata estuary (comprising of Montevideo and Buenos Aires), Cape Town and Rio de Janeiro. Recife, Pointe-Noire, Luanda and Benguela always returned probabilities equal or close to zero, in agreement with the findings of Onink et al. (2019) who argued that particles released in the northernmost part of the South Atlantic Ocean in forward simulations were able to cross the Equator and end up in the North Atlantic.

From the analysis of the 24 separated clusters of particles released during the *NIOZ 2019* simulation, it was possible to conclude that the internal variability of the ocean system might cause large discrepancies in the trajectories, and therefore identified sources, of particles released at relatively close distance but 12 days apart.

Future work

Overall, this work presented a new approach to study the land sources of microplastics from the outputs of Lagrangian simulations performed in backward mode. The algorithm developed to calculate the probabilities with that arbitrarily selected locations were identified as the sources of microplastics to the South Atlantic Subtropical Gyre was created in such a way to be a transferable method that could be used regardless of the study domain and the source locations that want to be addressed. The sources identified could at a later stage be investigated from a geographical or socio-economical perspective to quantify the amount of microplastic they are releasing to the Gyres and eventually to help with the implementation of better policies aimed to reduce microplastics pollution to the marine environment.

Future work is necessary to improve the soundness of the methodology developed in this study and to obtain more detailed results. While the calculation of probabilities based on trajectories obtained from Lagrangian simulations with a daily output provides an estimate of the sources on a time scale that captures the dynamic state of the system, a stronger approach would require to standardise the probabilities calculated regardless of the timestamp of the Lagrangian simulation's output. An additional term reproducing the sinking probability due to biofouling could be added to the current algorithm so that source probabilities would decrease with time at a rate that reflects the environmental conditions in the ocean. The work of Fazey and Ryan (2016) represents a starting point from which the implementation of sinking probability due to biofouling could be devised. Another factor that would reinforce the accuracy of the results obtained is the quantification of likely releases of (micro)plastics to the ocean from the sources investigated, so that it could be included as a *prior* to the calculation of source probabilities. This would increase the probabilities of those sources where more plastic is likely to be released to the marine environment compared to those where plastic waste is better managed. One database where information on mismanaged plastic waste is available is the Waste Atlas (2019; `http://www.atlas.d-waste.com`). Lastly, to be able to assess the probabilities of sources located relatively close to each other (e.g. Montevideo and Buenos Aires), each source could be attributed an area of influence. This would allow multiple sources to be the source of a particle with the same probability when the particle is located in the overlapping section of different areas of influence.

Bibliography

Andrady, A. L. (2011). Microplastics in the marine environment. *Marine pollution bulletin*, 62(8):1596–1605.

Arthur, C., Baker, J., and Bamford, H. (2009). Proceedings of the international research workshop on the occurrence, effects, and fate of microplastic marine debris. *Technical memorandum NOS-ORR-30*.

Chenillat, F., Blanke, B., Grima, N., Franks, P. J., Capet, X., and Rivière, P. (2015). Quantifying tracer dynamics in moving fluids: a combined eulerian-lagrangian approach. *Frontiers in Environmental Science*, 3:43.

Clarke, A. J. and Van Gorder, S. (2018). The relationship of near-surface flow, stokes drift and the wind stress. *Journal of Geophysical Research: Oceans*, 123(7):4680–4692.

Cózar, A., Echevarría, F., González-Gordillo, J. I., Irigoien, X., Úbeda, B., Hernández-León, S., Palma, Á. T., Navarro, S., García-de Lomas, J., Ruiz, A., et al. (2014). Plastic debris in the open ocean. *Proceedings of the National Academy of Sciences*, 111(28):10239–10244.

Delandmeter, P. and van Sebille, E. (2019). The parcels v2.0 lagrangian framework: new field interpolation schemes. *Geoscientific Model Development Discussions*, 2019:1–24.

Demographia (2019). Demographia world urban areas (15th ed.).

Derraik, J. G. (2002). The pollution of the marine environment by plastic debris: a review. *Marine pollution bulletin*, 44(9):842–852.

Do Sul, J. A. I., Costa, M. F., and Fillmann, G. (2014). Microplastics in the pelagic environment around oceanic islands of the western tropical atlantic ocean. *Water, Air, & Soil Pollution*, 225(7):2004.

Efron, B. (1992). Bootstrap methods: another look at the jackknife. In *Breakthroughs in statistics*, pages 569–593. Springer.

Eriksen, M., Lebreton, L. C., Carson, H. S., Thiel, M., Moore, C. J., Borerro, J. C., Galgani, F., Ryan, P. G., and Reisser, J. (2014). Plastic pollution in the world's oceans: more than 5 trillion plastic pieces weighing over 250,000 tons afloat at sea. *PloS one*, 9(12):e111913.

Fazey, F. M. and Ryan, P. G. (2016). Biofouling on buoyant marine plastics: An experimental study into the effect of size on surface longevity. *Environmental pollution*, 210:354–360.

Fraser, C. I., Morrison, A. K., Hogg, A. M., Macaya, E. C., van Sebille, E., Ryan, P. G., Padovan, A., Jack, C., Valdivia, N., and Waters, J. M. (2018). Antarctica's ecological isolation will be broken by storm-driven dispersal and warming. *Nature climate change*, 8(8):704.

Frias, J. and Nash, R. (2019). Microplastics: Finding a consensus on the definition. *Marine pollution bulletin*, 138:145–147.

Froyland, G., Stuart, R. M., and van Sebille, E. (2014). How well-connected is the surface of the global ocean? *Chaos: An Interdisciplinary Journal of Nonlinear Science*, 24(3):033126.

Galgani, F., Hanke, G., and Maes, T. (2015). Global distribution, composition and abundance of marine litter. In *Marine anthropogenic litter*, pages 29–56. Springer, Cham.

Gall, S. C. and Thompson, R. C. (2015). The impact of debris on marine life. *Marine pollution bulletin*, 92(1-2):170–179.

Geyer, R., Jambeck, J. R., and Law, K. L. (2017). Production, use, and fate of all plastics ever made. *Science advances*, 3(7):e1700782.

Isobe, A., Uchiyama-Matsumoto, K., Uchida, K., and Tokai, T. (2017). Microplastics in the southern ocean. *Marine pollution bulletin*, 114(1):623–626.

Jambeck, J., Hardesty, B. D., Brooks, A. L., Friend, T., Teleki, K., Fabres, J., Beaudoin, Y., Bamba, A., Francis, J., Ribbink, A. J., et al. (2018). Challenges and emerging solutions to the land-based plastic waste issue in africa. *Marine Policy*, 96:256–263.

Jambeck, J. R., Geyer, R., Wilcox, C., Siegler, T. R., Perryman, M., Andrady, A., Narayan, R., and Law, K. L. (2015). Plastic waste inputs from land into the ocean. *Science*, 347(6223):768–771.

Koelmans, A. A., Kooi, M., Law, K. L., and Van Sebille, E. (2017). All is not lost: deriving a top-down mass budget of plastic at sea. *Environmental Research Letters*, 12(11):114028.

Lange, M. and van Sebille, E. (2017). Parcels v0. 9: prototyping a lagrangian ocean analysis framework for the petascale age. *arXiv preprint arXiv:1707.05163*.

Lavers, J. L. and Bond, A. L. (2017). Exceptional and rapid accumulation of anthropogenic debris on one of the world's most remote and pristine islands. *Proceedings of the National Academy of Sciences*, 114(23):6052–6055.

Lebreton, L. and Andrady, A. (2019). Future scenarios of global plastic waste generation and disposal. *Palgrave Communications*, 5(1):6.

Lebreton, L. C., Van der Zwet, J., Damsteeg, J.-W., Slat, B., Andrady, A., and Reisser, J. (2017). River plastic emissions to the world's oceans. *Nature communications*, 8:15611.

Lebreton, L.-M., Greer, S., and Borrero, J. C. (2012). Numerical modelling of floating debris in the world's oceans. *Marine Pollution Bulletin*, 64(3):653–661.

Lett, C., Verley, P., Mullon, C., Parada, C., Brochier, T., Penven, P., and Blanke, B. (2008). A lagrangian tool for modelling ichthyoplankton dynamics. *Environmental Modelling & Software*, 23(9):1210–1214.

Lindsay, R. and Stern, H. (2004). A new lagrangian model of arctic sea ice. *Journal of physical oceanography*, 34(1):272–283.

Madec, G. and the NEMO team (2008). NEMO ocean engine. *Note du Pôle de modélisation*, 27:ISSN No 1288–1619.

Maximenko, N., Hafner, J., and Niiler, P. (2012). Pathways of marine debris derived from trajectories of lagrangian drifters. *Marine pollution bulletin*, 65(1-3):51–62.

Niebler, H.-S., Arz, H., Donner, B., Mulitza, S., Pätzold, J., and Wefer, G. (2003). Sea surface temperatures in the equatorial and south atlantic ocean during the last glacial maximum (23–19 ka). *Paleoceanography*, 18(3).

North, E. W., Adams, E. E., Schlag, Z., Sherwood, C. R., He, R., Hyun, K. H., and Socolofsky, S. A. (2011). Simulating oil droplet dispersal from the deepwater horizon spill with a lagrangian approach. *Geophys. Monogr. Ser*, 195:217–226.

Obbard, R. W., Sadri, S., Wong, Y. Q., Khitun, A. A., Baker, I., and Thompson, R. C. (2014). Global warming releases microplastic legacy frozen in arctic sea ice. *Earth's Future*, 2(6):315–320.

Oehlmann, J., Schulte-Oehlmann, U., Kloas, W., Jagnytsch, O., Lutz, I., Kusk, K. O., Wollenberger, L., Santos, E. M., Paull, G. C., Van Look, K. J., et al. (2009). A critical analysis of the biological impacts of plasticizers on wildlife. *Philosophical Transactions of the Royal Society B: Biological Sciences*, 364(1526):2047–2062.

Onink, V., Wichmann, D., Delandmeter, P., and van Sebille, E. (2019). The role of ekman currents, geostrophy, and stokes drift in the accumulation of floating microplastic. *Journal of Geophysical Research: Oceans*, 124(3):1474–1490.

Parker, W. S. (2016). Reanalyses and observations: What's the difference? *Bulletin of the American Meteorological Society*, 97(9):1565–1572.

PlasticsEurope (2013). Plastics-the facts 2013. *An analysis of European latest plastics production, demand and waste data.*

PlasticsEurope (2018). Plastics-the facts 2018. *An analysis of European latest plastics production, demand and waste data.*

Rae, D. (1991). Agulhas retroflection rings in the south atlantic ocean: an overview. *South African Journal of Marine Science*, 11(1):327–344.

Rampal, P., Bouillon, S., Ólason, E., and Morlighem, M. (2016). nextsim: a new lagrangian sea ice model.

Reboita, M. S., Ambrizzi, T., Silva, B., Pinheiro, R., and Da Rocha, R. P. (2019). The south atlantic subtropical anticyclone: Present and future climate. *Frontiers in Earth Science*, 7:8.

Röhrs, J., Christensen, K. H., Hole, L. R., Broström, G., Drivdal, M., and Sundby, S. (2012). Observation-based evaluation of surface wave effects on currents and trajectory forecasts. *Ocean Dynamics*, 62(10-12):1519–1533.

Ryan, P. and Watkins, B. (1988). Accumulation of stranded plastic objects and other artefacts at inaccessible island, central south atlantic ocean.

Ryan, P. G. (2014). Litter survey detects the south atlantic 'garbage patch'. *Marine Pollution Bulletin*, 79(1-2):220–224.

Thompson, R. C., Moore, C. J., Vom Saal, F. S., and Swan, S. H. (2009). Plastics, the environment and human health: current consensus and future trends. *Philosophical Transactions of the Royal Society B: Biological Sciences*, 364(1526):2153–2166.

van Sebille, E. (2015). The oceans' accumulating plastic garbage.

van Sebille, E., England, M. H., and Froyland, G. (2012). Origin, dynamics and evolution of ocean garbage patches from observed surface drifters. *Environmental Research Letters*, 7(4):044040.

van Sebille, E., Griffies, S. M., Abernathey, R., Adams, T. P., Berloff, P., Biastoch, A., Blanke, B., Chassignet, E. P., Cheng, Y., Cotter, C. J., et al. (2018). Lagrangian ocean analysis: Fundamentals and practices. *Ocean Modelling*, 121:49–75.

van Sebille, E., Wilcox, C., Lebreton, L., Maximenko, N., Hardesty, B. D., Van Franeker, J. A., Eriksen, M., Siegel, D., Galgani, F., and Law, K. L. (2015). A global inventory of small floating plastic debris. *Environmental Research Letters*, 10(12):124006.

Wichmann, D., Delandmeter, P., Dijkstra, H., and van Sebille, E. (2019). Mixing of passive tracers at the ocean surface and its implications for plastic transport modellnig. *Manuscript submitted for publication.*

Woodall, L. C., Sanchez-Vidal, A., Canals, M., Paterson, G. L., Coppock, R., Sleight, V., Calafat, A., Rogers, A. D., Narayanaswamy, B. E., and Thompson, R. C. (2014). The deep sea is a major sink for microplastic debris. *Royal Society open science*, 1(4):140317.

Wright, S. L. and Kelly, F. J. (2017). Plastic and human health: a micro issue? *Environmental science & technology*, 51(12):6634–6647.

A. Additional Figures

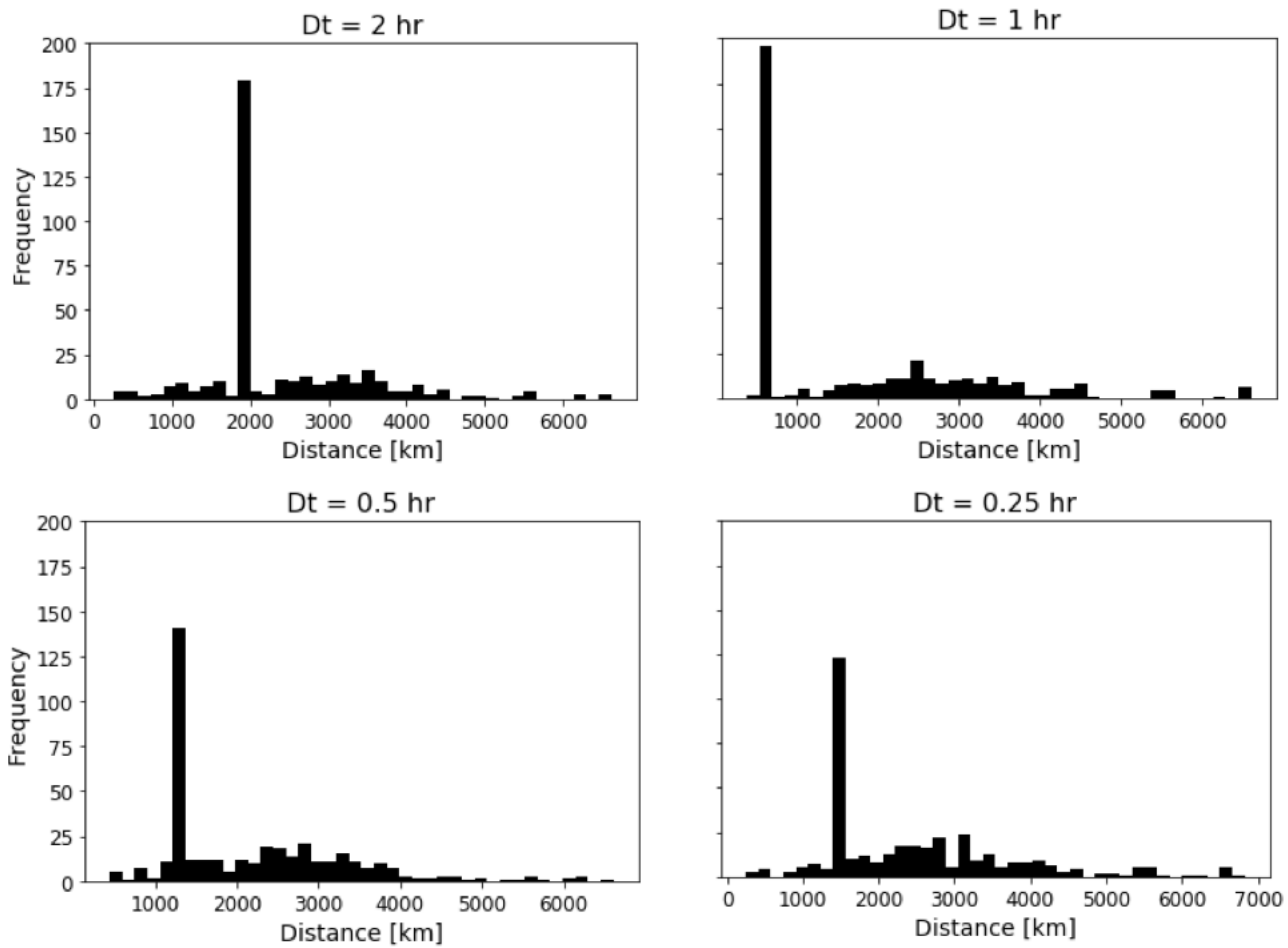

Figure A.1: Haversine distances calculated between the initial and final positions of corresponding particle trajectories obtained from simulations performed with different integration time steps. All distances are grouped in 40 bins. Please note the different values on the x-axis.

B. Probability Tables

Sampling Location #	Luanda	Benguela	Cape Town	Pointe Noire	Rio de Janeiro	Salvador	Recife	Buenos Aires	Montevideo	Rest
1	0.000	0.000	92.351	0.000	0.000	0.000	0.000	0.003	0.007	7.639
	0.000	0.000	0.169	0.000	0.000	0.000	0.000	0.003	0.007	
2	0.000	0.000	3.388	0.000	0.122	0.294	0.000	0.436	5.177	90.583
	0.000	0.000	0.074	0.000	0.038	0.119	0.000	0.155	0.675	
3	0.000	0.000	0.895	0.000	0.541	0.370	0.000	3.019	16.188	78.987
	0.000	0.000	0.166	0.000	0.122	0.121	0.000	0.400	1.057	
4	0.000	0.000	0.348	0.000	0.236	0.295	0.000	2.671	12.262	84.188
	0.000	0.000	0.059	0.000	0.051	0.110	0.000	0.401	0.952	
5	0.000	0.000	0.763	0.000	0.311	0.470	0.000	2.452	12.697	83.307
	0.000	0.000	0.144	0.000	0.054	0.144	0.000	0.363	0.958	
6	0.000	0.000	0.324	0.000	0.345	0.099	0.000	1.122	11.200	86.910
	0.000	0.000	0.049	0.000	0.087	0.041	0.000	0.256	0.904	
7	0.000	0.000	0.659	0.000	0.448	0.156	0.000	1.516	12.165	85.056
	0.000	0.000	0.161	0.000	0.125	0.071	0.000	0.274	0.975	
8	0.000	0.000	0.491	0.000	0.309	0.319	0.000	1.581	11.680	85.620
	0.000	0.000	0.079	0.000	0.058	0.115	0.000	0.296	0.927	
9	0.000	0.000	0.618	0.000	0.257	0.300	0.001	1.137	9.135	88.552
	0.000	0.000	0.148	0.000	0.053	0.113	0.001	0.256	0.880	
10	0.000	0.000	0.683	0.000	0.331	0.176	0.000	1.524	10.631	86.655
	0.000	0.000	0.161	0.000	0.076	0.094	0.000	0.282	0.926	
11	0.000	0.000	0.476	0.000	0.139	0.176	0.000	1.414	12.139	85.656
	0.000	0.000	0.126	0.000	0.025	0.079	0.000	0.265	1.008	
12	0.000	0.000	0.560	0.000	0.473	0.218	0.000	1.057	10.007	87.685
	0.000	0.000	0.090	0.000	0.107	0.089	0.000	0.223	0.838	
13	0.000	0.000	0.417	0.000	0.403	0.216	0.000	1.617	9.954	87.393
	0.000	0.000	0.085	0.000	0.091	0.098	0.000	0.287	0.885	
14	0.000	0.000	0.218	0.000	0.286	0.032	0.000	0.774	7.910	90.780
	0.000	0.000	0.104	0.000	0.082	0.021	0.000	0.193	0.791	
15	0.000	0.000	0.521	0.000	0.347	0.061	0.000	0.993	9.386	88.692
	0.000	0.000	0.154	0.000	0.109	0.031	0.000	0.221	0.868	
16	0.000	0.000	0.295	0.000	0.194	0.075	0.000	0.528	7.060	91.848
	0.000	0.000	0.096	0.000	0.071	0.060	0.000	0.135	0.765	
17	0.000	0.000	0.536	0.000	0.304	0.025	0.000	0.689	7.473	90.973
	0.000	0.000	0.156	0.000	0.109	0.012	0.000	0.184	0.760	
18	0.000	0.000	0.424	0.000	0.287	0.075	0.000	0.721	8.567	89.926
	0.000	0.000	0.105	0.000	0.076	0.041	0.000	0.181	0.830	
19	0.000	0.000	0.581	0.000	0.149	0.331	0.000	0.604	9.478	88.857
	0.000	0.000	0.135	0.000	0.031	0.134	0.000	0.165	0.836	
20	0.000	0.000	0.715	0.000	0.380	0.314	0.000	1.243	12.002	85.346
	0.000	0.000	0.149	0.000	0.104	0.104	0.000	0.235	0.971	
21	0.000	0.000	0.714	0.000	0.358	0.222	0.000	1.482	10.600	86.624
	0.000	0.000	0.184	0.000	0.100	0.074	0.000	0.274	0.940	
22	0.000	0.000	0.839	0.000	0.317	0.268	0.000	2.864	14.125	81.587
	0.000	0.000	0.165	0.000	0.060	0.101	0.000	0.398	1.035	
23	0.000	0.000	0.769	0.000	0.502	0.534	0.000	2.668	11.909	83.618
	0.000	0.000	0.119	0.000	0.106	0.139	0.000	0.415	0.961	
24	0.000	0.000	0.446	0.000	0.213	0.305	0.000	2.415	8.674	87.947
	0.000	0.000	0.064	0.000	0.047	0.095	0.000	0.375	0.781	

Table B.1: Probabilities calculated for each of the 24 *NIOZ 2019* sampling locations using the exponential distribution with $\beta = 25$ km. For each sampling location the first row represents the mean and the second the standard deviation obtained from bootstrapping.

Sampling Location #	Luanda	Benguela	Cape Town	Pointe Noire	Rio de Janeiro	Salvador	Recife	Buenos Aires	Montevideo	Rest
1	0.000	0.000	100.000	0.000	0.000	0.000	0.000	0.000	0.000	0.000
	0.000	0.000	0.000	0.000	0.000	0.000	0.000	0.000	0.000	
2	0.000	0.000	98.789	0.000	0.047	0.003	0.000	0.010	0.139	1.012
	0.000	0.000	0.027	0.000	0.007	0.001	0.000	0.002	0.013	
3	0.000	0.000	14.728	0.000	13.717	0.675	0.004	3.172	31.332	36.371
	0.000	0.000	0.294	0.000	0.752	0.129	0.001	0.286	1.111	
4	0.000	0.000	12.999	0.000	9.827	0.394	0.002	2.851	27.399	46.528
	0.000	0.000	0.641	0.000	0.718	0.081	0.001	0.267	1.178	
5	0.000	0.000	12.170	0.000	13.029	0.775	0.011	2.943	35.443	35.629
	0.000	0.000	0.691	0.000	0.799	0.150	0.005	0.265	1.243	
6	0.000	0.000	20.171	0.000	11.163	0.434	0.002	1.018	28.215	38.997
	0.000	0.000	0.789	0.000	0.738	0.089	0.001	0.134	1.176	
7	0.000	0.000	5.420	0.000	13.337	0.716	0.013	1.486	31.364	47.665
	0.000	0.000	0.529	0.000	0.824	0.138	0.006	0.207	1.252	
8	0.000	0.000	7.050	0.000	17.170	0.835	0.007	1.614	30.000	43.324
	0.000	0.000	0.594	0.000	0.945	0.153	0.002	0.209	1.240	
9	0.000	0.000	10.680	0.000	13.634	1.068	0.012	0.651	26.609	47.345
	0.000	0.000	0.757	0.000	0.849	0.178	0.004	0.083	1.228	
10	0.000	0.000	6.847	0.000	14.404	0.915	0.007	0.925	26.926	49.977
	0.000	0.000	0.572	0.000	0.821	0.164	0.004	0.163	1.232	
11	0.000	0.000	4.598	0.000	11.683	0.701	0.008	1.054	31.230	50.726
	0.000	0.000	0.469	0.000	0.744	0.138	0.003	0.167	1.279	
12	0.000	0.000	8.507	0.000	16.139	0.950	0.014	0.985	26.099	47.305
	0.000	0.000	0.637	0.000	0.890	0.167	0.005	0.137	1.156	
13	0.000	0.000	7.205	0.000	17.392	1.104	0.016	0.710	26.914	46.658
	0.000	0.000	0.573	0.000	0.896	0.193	0.006	0.111	1.214	
14	0.000	0.000	6.795	0.000	9.537	0.621	0.006	0.357	20.382	62.303
	0.000	0.000	0.579	0.000	0.714	0.130	0.002	0.066	1.070	
15	0.000	0.000	10.483	0.000	13.622	0.693	0.005	0.526	21.327	53.343
	0.000	0.000	0.731	0.000	0.807	0.130	0.001	0.084	1.112	
16	0.000	0.000	6.485	0.000	9.872	0.918	0.019	0.522	21.418	60.766
	0.000	0.000	0.581	0.000	0.663	0.186	0.006	0.088	1.126	
17	0.000	0.000	7.215	0.000	12.463	0.825	0.011	0.598	22.785	56.103
	0.000	0.000	0.572	0.000	0.745	0.176	0.004	0.102	1.152	
18	0.000	0.000	6.355	0.000	11.715	0.949	0.014	1.011	28.253	51.702
	0.000	0.000	0.583	0.000	0.755	0.168	0.006	0.154	1.229	
19	0.000	0.000	7.146	0.000	13.929	0.989	0.015	0.499	28.095	49.326
	0.000	0.000	0.603	0.000	0.810	0.168	0.007	0.068	1.188	
20	0.000	0.000	8.313	0.000	16.447	1.457	0.007	1.281	30.759	41.735
	0.000	0.000	0.623	0.000	0.900	0.239	0.002	0.168	1.249	
21	0.000	0.000	6.092	0.000	13.288	1.099	0.022	1.208	26.765	51.525
	0.000	0.000	0.555	0.000	0.820	0.179	0.008	0.180	1.219	
22	0.000	0.000	7.792	0.000	12.364	0.530	0.003	3.855	35.945	39.511
	0.000	0.000	0.517	0.000	0.793	0.105	0.001	0.328	1.218	
23	0.000	0.000	15.954	0.000	14.000	0.819	0.008	2.113	30.216	36.890
	0.000	0.000	0.680	0.000	0.820	0.129	0.003	0.212	1.162	
24	0.000	0.000	51.088	0.000	5.092	0.291	0.002	1.641	14.687	27.199
	0.000	0.000	0.928	0.000	0.486	0.073	0.001	0.183	0.820	

Table B.2: Probabilities calculated for each of the 24 *NIOZ 2019* sampling locations using the exponential distribution with $\beta = 100$ km. For each sampling location the first row represents the mean and the second the standard deviation obtained from bootstrapping.

	NIOZ 2019	Bootstrap Mean	Bootstrap St Dev
Luanda_2.5	0.000	0.000	0.000
Luanda_10	0.000	0.000	0.000
Luanda_14.3	0.000	0.000	0.000
Luanda_25	0.000	0.000	0.000
Luanda_100	0.000	0.000	0.000
Luanda_143	0.000	0.000	0.000
Luanda_250	0.000	0.000	0.000
Benguela_2.5	0.000	0.000	0.000
Benguela_10	0.000	0.000	0.000
Benguela_14.3	0.000	0.000	0.000
Benguela_25	0.000	0.000	0.000
Benguela_100	0.000	0.000	0.000
Benguela_143	0.002	0.002	0.000
Beguela_250	0.055	0.055	0.002
Cape Town_2.5	0.010	0.010	0.006
Cape Town_10	1.309	1.310	0.043
Cape Town_14.3	2.577	2.577	0.079
Cape Town_25	4.502	4.502	0.120
Cape Town_100	18.459	18.465	0.209
Cape Town_143	26.852	26.858	0.237
Cape Town_250	47.586	47.592	0.270
Pointe Noire_2.5	0.000	0.000	0.000
Pointe Noire_10	0.000	0.000	0.000
Pointe Noire_14.3	0.000	0.000	0.000
Pointe Noire_25	0.000	0.000	0.000
Pointe Noire_100	0.000	0.000	0.000
Pointe Noire_143	0.000	0.000	0.000
Pointe Noire_250	0.000	0.000	0.000
Buenos Aires_2.5	3.607	3.605	0.105
Buenos Aires_10	5.476	5.472	0.131
Buenos Aires_14.3	4.198	4.194	0.107
Buenos Aires_25	1.437	1.435	0.054
Buenos Aires_100	1.294	1.295	0.036
Buenos Aires_143	2.040	2.040	0.057
Buenos Aires_250	0.286	0.286	0.011
Rio de Janeiro_2.5	0.000	0.000	0.000
Rio de Janeiro_10	0.009	0.009	0.004
Rio de Janeiro_14.3	0.032	0.031	0.007
Rio de Janeiro_25	0.302	0.301	0.017
Rio de Janeiro_100	11.827	11.828	0.160
Rio de Janeiro_143	16.064	16.066	0.187
Rio de Janeiro_250	27.173	27.172	0.229
Salvador_2.5	0.000	0.000	0.000
Salvador_10	0.014	0.014	0.002
Salvador_14.3	0.048	0.048	0.006
Salvador_25	0.223	0.222	0.019
Salvador_100	0.740	0.738	0.030
Salvador_143	0.280	0.279	0.014
Salvador_250	0.150	0.150	0.005
Recife_2.5	0.000	0.000	0.000
Recife_10	0.000	0.000	0.000
Recife_14.3	0.000	0.000	0.000
Recife_25	0.000	0.000	0.000
Recife_100	0.009	0.009	0.001
Recife_143	0.003	0.003	0.000
Recife_250	0.008	0.008	0.000
Montevideo_2.5	0.747	0.748	0.034
Montevideo_10	2.780	2.782	0.080
Montevideo_14.3	5.101	5.101	0.115
Montevideo_25	10.016	10.014	0.182
Montevideo_100	25.093	25.099	0.239
Montevideo_143	31.677	31.682	0.254
Montevideo_250	21.729	21.725	0.212

Table B.3: Probabilities calculated for *NIOZ 2019* from the exponential distribution when considering the entire 5-year simulation.

	NIOZ 2019 - 2.5 yrs	Bootstrap Mean	Bootstrap St Dev
Luanda_2.5	0.000	0.000	0.000
Luanda_10	0.000	0.000	0.000
Luanda_14.3	0.000	0.000	0.000
Luanda_25	0.000	0.000	0.000
Luanda_100	0.000	0.000	0.000
Luanda_143	0.000	0.000	0.000
Luanda_250	0.000	0.000	0.000
Benguela_2.5	0.000	0.000	0.000
Benguela_10	0.000	0.000	0.000
Benguela_14.3	0.000	0.000	0.000
Benguela_25	0.000	0.000	0.000
Benguela_100	0.000	0.000	0.000
Benguela_143	0.000	0.000	0.000
Beguela_250	0.022	0.022	0.001
Cape Town_2.5	0.001	0.001	0.000
Cape Town_10	1.256	1.259	0.042
Cape Town_14.3	2.466	2.469	0.079
Cape Town_25	3.992	3.998	0.120
Cape Town_100	13.748	13.758	0.193
Cape Town_143	22.098	22.113	0.228
Cape Town_250	44.727	44.743	0.277
Pointe Noire_2.5	0.000	0.000	0.000
Pointe Noire_10	0.000	0.000	0.000
Pointe Noire_14.3	0.000	0.000	0.000
Pointe Noire_25	0.000	0.000	0.000
Pointe Noire_100	0.000	0.000	0.000
Pointe Noire_143	0.000	0.000	0.000
Pointe Noire_250	0.000	0.000	0.000
Buenos Aires_2.5	2.467	2.464	0.088
Buenos Aires_10	3.005	3.003	0.099
Buenos Aires_14.3	2.383	2.382	0.084
Buenos Aires_25	0.959	0.959	0.049
Buenos Aires_100	0.763	0.761	0.026
Buenos Aires_143	1.159	1.158	0.034
Buenos Aires_250	0.196	0.196	0.008
Rio de Janeiro_2.5	0.000	0.000	0.000
Rio de Janeiro_10	0.008	0.008	0.003
Rio de Janeiro_14.3	0.021	0.021	0.006
Rio de Janeiro_25	0.160	0.160	0.012
Rio de Janeiro_100	6.906	6.902	0.127
Rio de Janeiro_143	9.507	9.504	0.139
Rio de Janeiro_250	21.251	21.242	0.202
Salvador_2.5	0.000	0.000	0.000
Salvador_10	0.012	0.012	0.002
Salvador_14.3	0.042	0.042	0.005
Salvador_25	0.186	0.186	0.017
Salvador_100	0.240	0.240	0.015
Salvador_143	0.051	0.051	0.003
Salvador_250	0.075	0.075	0.003
Recife_2.5	0.000	0.000	0.000
Recife_10	0.000	0.000	0.000
Recife_14.3	0.000	0.000	0.000
Recife_25	0.000	0.000	0.000
Recife_100	0.001	0.001	0.000
Recife_143	0.000	0.000	0.000
Recife_250	0.002	0.002	0.000
Montevideo_2.5	0.166	0.166	0.017
Montevideo_10	1.603	1.599	0.061
Montevideo_14.3	2.957	2.952	0.085
Montevideo_25	5.602	5.594	0.136
Montevideo_100	16.543	16.530	0.202
Montevideo_143	22.628	22.610	0.224
Montevideo_250	18.979	18.965	0.200

Table B.4: Probabilities calculated for *NIOZ 2019* from the exponential distribution when considering only the first 2.5 years of the simulation.

	NIOZ 2019	Bootstrap Mean	Bootstrap St Dev
Luanda_2.5	0.000	0.000	0.000
Luanda_10	0.000	0.000	0.000
Luanda_14.3	0.000	0.000	0.000
Luanda_25	0.000	0.000	0.000
Luanda_100	0.000	0.000	0.000
Luanda_143	0.000	0.000	0.000
Luanda_250	0.000	0.000	0.000
Benguela_2.5	0.000	0.000	0.000
Benguela_10	0.000	0.000	0.000
Benguela_14.3	0.000	0.000	0.000
Benguela_25	0.000	0.000	0.000
Benguela_100	0.000	0.000	0.000
Benguela_143	0.000	0.000	0.000
Beguela_250	0.000	0.000	0.000
Cape Town_2.5	0.005	0.006	0.004
Cape Town_10	0.372	0.372	0.019
Cape Town_14.3	1.953	1.951	0.065
Cape Town_25	4.023	4.021	0.123
Cape Town_100	13.912	13.912	0.209
Cape Town_143	16.055	16.058	0.228
Cape Town_250	30.081	30.085	0.265
Pointe Noire_2.5	0.000	0.000	0.000
Pointe Noire_10	0.000	0.000	0.000
Pointe Noire_14.3	0.000	0.000	0.000
Pointe Noire_25	0.000	0.000	0.000
Pointe Noire_100	0.000	0.000	0.000
Pointe Noire_143	0.000	0.000	0.000
Pointe Noire_250	0.000	0.000	0.000
Buenos Aires_2.5	3.296	3.296	0.104
Buenos Aires_10	5.325	5.322	0.134
Buenos Aires_14.3	5.307	5.303	0.132
Buenos Aires_25	3.142	3.138	0.098
Buenos Aires_100	0.000	0.000	0.000
Buenos Aires_143	0.000	0.000	0.000
Buenos Aires_250	0.099	0.099	0.010
Rio de Janeiro_2.5	0.000	0.000	0.000
Rio de Janeiro_10	0.003	0.003	0.002
Rio de Janeiro_14.3	0.010	0.010	0.005
Rio de Janeiro_25	0.034	0.034	0.009
Rio de Janeiro_100	7.169	7.167	0.145
Rio de Janeiro_143	10.299	10.292	0.171
Rio de Janeiro_250	12.477	12.467	0.194
Salvador_2.5	0.000	0.000	0.000
Salvador_10	0.001	0.001	0.000
Salvador_14.3	0.014	0.014	0.003
Salvador_25	0.111	0.112	0.015
Salvador_100	0.792	0.791	0.044
Salvador_143	0.695	0.693	0.040
Salvador_250	0.148	0.148	0.016
Recife_2.5	0.000	0.000	0.000
Recife_10	0.000	0.000	0.000
Recife_14.3	0.000	0.000	0.000
Recife_25	0.000	0.000	0.000
Recife_100	0.000	0.000	0.000
Recife_143	0.001	0.000	0.000
Recife_250	0.000	0.000	0.000
Montevideo_2.5	0.619	0.619	0.033
Montevideo_10	2.154	2.156	0.080
Montevideo_14.3	2.935	2.938	0.091
Montevideo_25	6.945	6.949	0.150
Montevideo_100	14.954	14.950	0.212
Montevideo_143	23.052	23.045	0.240
Montevideo_250	33.247	33.239	0.278

Table B.5: Probabilities calculated for *NIOZ 2019* from the quadratic distribution when considering the entire 5-year simulation.

	NIOZ 2019 - 2.5 yrs	**Bootstrap Mean**	**Bootstrap St Dev**
Luanda_2.5	0.000	0.000	0.000
Luanda_10	0.000	0.000	0.000
Luanda_14.3	0.000	0.000	0.000
Luanda_25	0.000	0.000	0.000
Luanda_100	0.000	0.000	0.000
Luanda_143	0.000	0.000	0.000
Luanda_250	0.000	0.000	0.000
Benguela_2.5	0.000	0.000	0.000
Benguela_10	0.000	0.000	0.000
Benguela_14.3	0.000	0.000	0.000
Benguela_25	0.000	0.000	0.000
Benguela_100	0.000	0.000	0.000
Benguela_143	0.000	0.000	0.000
Beguela_250	0.000	0.000	0.000
Cape Town_2.5	0.000	0.000	0.000
Cape Town_10	0.344	0.344	0.017
Cape Town_14.3	1.895	1.895	0.065
Cape Town_25	3.881	3.882	0.121
Cape Town_100	9.355	9.364	0.184
Cape Town_143	11.145	11.154	0.203
Cape Town_250	24.482	24.499	0.261
Pointe Noire_2.5	0.000	0.000	0.000
Pointe Noire_10	0.000	0.000	0.000
Pointe Noire_14.3	0.000	0.000	0.000
Pointe Noire_25	0.000	0.000	0.000
Pointe Noire_100	0.000	0.000	0.000
Pointe Noire_143	0.000	0.000	0.000
Pointe Noire_250	0.000	0.000	0.000
Buenos Aires_2.5	2.321	2.319	0.091
Buenos Aires_10	3.241	3.237	0.114
Buenos Aires_14.3	2.850	2.848	0.102
Buenos Aires_25	1.793	1.793	0.076
Buenos Aires_100	0.000	0.000	0.000
Buenos Aires_143	0.000	0.000	0.000
Buenos Aires_250	0.073	0.073	0.008
Rio de Janeiro_2.5	0.000	0.000	0.000
Rio de Janeiro_10	0.003	0.003	0.002
Rio de Janeiro_14.3	0.010	0.010	0.005
Rio de Janeiro_25	0.025	0.026	0.009
Rio de Janeiro_100	4.378	4.378	0.112
Rio de Janeiro_143	6.264	6.266	0.141
Rio de Janeiro_250	7.300	7.303	0.149
Salvador_2.5	0.000	0.000	0.000
Salvador_10	0.001	0.001	0.000
Salvador_14.3	0.013	0.013	0.003
Salvador_25	0.098	0.099	0.015
Salvador_100	0.412	0.412	0.032
Salvador_143	0.140	0.141	0.013
Salvador_250	0.002	0.002	0.001
Recife_2.5	0.000	0.000	0.000
Recife_10	0.000	0.000	0.000
Recife_14.3	0.000	0.000	0.000
Recife_25	0.000	0.000	0.000
Recife_100	0.000	0.000	0.000
Recife_143	0.000	0.000	0.000
Recife_250	0.000	0.000	0.000
Montevideo_2.5	0.105	0.105	0.014
Montevideo_10	1.011	1.011	0.053
Montevideo_14.3	1.830	1.828	0.070
Montevideo_25	3.969	3.965	0.113
Montevideo_100	8.507	8.498	0.162
Montevideo_143	14.666	14.659	0.202
Montevideo_250	23.193	23.178	0.248

Table B.6: Probabilities calculated for *NIOZ 2019* from the quadratic distribution when considering only the first 2.5 years of the simulation.

	van Sebille et al. (2015)	Bootstrap Mean	Bootstrap St Dev
Luanda_2.5	0.000	0.000	0.000
Luanda_10	0.000	0.000	0.000
Luanda_14.3	0.000	0.000	0.000
Luanda_25	0.000	0.000	0.000
Luanda_100	0.000	0.000	0.000
Luanda_143	0.001	0.001	0.000
Luanda_250	0.011	0.011	0.002
Benguela_2.5	0.000	0.000	0.000
Benguela_10	0.000	0.000	0.000
Benguela_14.3	0.000	0.000	0.000
Benguela_25	0.000	0.000	0.000
Benguela_100	0.011	0.011	0.001
Benguela_143	0.166	0.166	0.008
Beguela_250	1.962	1.963	0.044
Cape Town_2.5	0.029	0.029	0.009
Cape Town_10	0.136	0.135	0.018
Cape Town_14.3	0.268	0.267	0.021
Cape Town_25	1.203	1.203	0.039
Cape Town_100	16.236	16.238	0.185
Cape Town_143	21.990	21.995	0.202
Cape Town_250	28.024	28.033	0.217
Pointe Noire_2.5	0.000	0.000	0.000
Pointe Noire_10	0.000	0.000	0.000
Pointe Noire_14.3	0.000	0.000	0.000
Pointe Noire_25	0.000	0.000	0.000
Pointe Noire_100	0.000	0.000	0.000
Pointe Noire_143	0.001	0.001	0.000
Pointe Noire_250	0.051	0.051	0.004
Buenos Aires_2.5	0.639	0.640	0.036
Buenos Aires_10	2.248	2.249	0.083
Buenos Aires_14.3	1.867	1.867	0.068
Buenos Aires_25	0.663	0.663	0.030
Buenos Aires_100	1.120	1.118	0.033
Buenos Aires_143	1.342	1.341	0.034
Buenos Aires_250	1.042	1.042	0.052
Rio de Janeiro_2.5	0.000	0.000	0.000
Rio de Janeiro_10	0.001	0.001	0.000
Rio de Janeiro_14.3	0.008	0.008	0.002
Rio de Janeiro_25	0.098	0.098	0.009
Rio de Janeiro_100	7.080	7.080	0.115
Rio de Janeiro_143	12.477	12.477	0.150
Rio de Janeiro_250	30.086	30.082	0.219
Salvador_2.5	0.000	0.000	0.000
Salvador_10	0.013	0.013	0.002
Salvador_14.3	0.036	0.036	0.005
Salvador_25	0.137	0.137	0.014
Salvador_100	0.582	0.584	0.024
Salvador_143	1.132	1.134	0.030
Salvador_250	2.912	2.914	0.070
Recife_2.5	0.000	0.000	0.000
Recife_10	0.000	0.000	0.000
Recife_14.3	0.000	0.000	0.000
Recife_25	0.000	0.000	0.000
Recife_100	0.102	0.102	0.004
Recife_143	0.616	0.615	0.021
Recife_250	2.889	2.885	0.082
Montevideo_2.5	0.283	0.282	0.021
Montevideo_10	1.387	1.387	0.059
Montevideo_14.3	2.345	2.345	0.077
Montevideo_25	4.750	4.750	0.115
Montevideo_100	16.268	16.271	0.189
Montevideo_143	22.483	22.479	0.215
Montevideo_250	20.772	20.763	0.201

Table B.7: Probabilities calculated for *van Sebille et al. (2015)* from the exponential distribution when considering the entire 5-year simulation.

	van Sebille et al. (2015) - 2.5 yrs	Bootstrap Mean	Bootstrap St Dev
Luanda_2.5	0.000	0.000	0.000
Luanda_10	0.000	0.000	0.000
Luanda_14.3	0.000	0.000	0.000
Luanda_25	0.000	0.000	0.000
Luanda_100	0.000	0.000	0.000
Luanda_143	0.001	0.001	0.000
Luanda_250	0.011	0.011	0.002
Benguela_2.5	0.000	0.000	0.000
Benguela_10	0.000	0.000	0.000
Benguela_14.3	0.000	0.000	0.000
Benguela_25	0.000	0.000	0.000
Benguela_100	0.011	0.011	0.001
Benguela_143	0.166	0.166	0.008
Beguela_250	1.960	1.962	0.043
Cape Town_2.5	0.029	0.029	0.009
Cape Town_10	0.136	0.135	0.018
Cape Town_14.3	0.266	0.266	0.021
Cape Town_25	1.188	1.189	0.038
Cape Town_100	15.988	15.989	0.183
Cape Town_143	21.689	21.691	0.199
Cape Town_250	27.687	27.679	0.222
Pointe Noire_2.5	0.000	0.000	0.000
Pointe Noire_10	0.000	0.000	0.000
Pointe Noire_14.3	0.000	0.000	0.000
Pointe Noire_25	0.000	0.000	0.000
Pointe Noire_100	0.000	0.000	0.000
Pointe Noire_143	0.001	0.001	0.000
Pointe Noire_250	0.051	0.051	0.004
Buenos Aires_2.5	0.426	0.427	0.029
Buenos Aires_10	1.588	1.587	0.073
Buenos Aires_14.3	1.295	1.294	0.059
Buenos Aires_25	0.434	0.433	0.025
Buenos Aires_100	0.889	0.890	0.026
Buenos Aires_143	1.189	1.189	0.033
Buenos Aires_250	0.992	0.990	0.050
Rio de Janeiro_2.5	0.000	0.000	0.000
Rio de Janeiro_10	0.001	0.001	0.000
Rio de Janeiro_14.3	0.004	0.004	0.001
Rio de Janeiro_25	0.060	0.060	0.006
Rio de Janeiro_100	6.539	6.541	0.108
Rio de Janeiro_143	12.008	12.010	0.153
Rio de Janeiro_250	29.404	29.402	0.224
Salvador_2.5	0.000	0.000	0.000
Salvador_10	0.013	0.013	0.002
Salvador_14.3	0.036	0.035	0.005
Salvador_25	0.134	0.133	0.014
Salvador_100	0.580	0.580	0.025
Salvador_143	1.132	1.131	0.030
Salvador_250	2.908	2.909	0.072
Recife_2.5	0.000	0.000	0.000
Recife_10	0.000	0.000	0.000
Recife_14.3	0.000	0.000	0.000
Recife_25	0.000	0.000	0.000
Recife_100	0.102	0.102	0.004
Recife_143	0.616	0.617	0.021
Recife_250	2.888	2.893	0.082
Montevideo_2.5	0.279	0.279	0.020
Montevideo_10	1.327	1.327	0.057
Montevideo_14.3	2.207	2.206	0.075
Montevideo_25	4.354	4.350	0.111
Montevideo_100	14.540	14.543	0.180
Montevideo_143	20.435	20.443	0.207
Montevideo_250	19.472	19.485	0.205

Table B.8: Probabilities calculated for *van Sebille et al. (2015)* from the exponential distribution when considering only the first 2.5 years of the simulation.

	van Sebille et al. (2015)	Bootstrap Mean	Bootstrap St Dev
Luanda_2.5	0.000	0.000	0.000
Luanda_10	0.000	0.000	0.000
Luanda_14.3	0.000	0.000	0.000
Luanda_25	0.000	0.000	0.000
Luanda_100	0.000	0.000	0.000
Luanda_143	0.000	0.000	0.000
Luanda_250	0.000	0.000	0.000
Benguela_2.5	0.000	0.000	0.000
Benguela_10	0.000	0.000	0.000
Benguela_14.3	0.000	0.000	0.000
Benguela_25	0.000	0.000	0.000
Benguela_100	0.000	0.000	0.000
Benguela_143	0.000	0.000	0.000
Beguela_250	0.027	0.027	0.008
Cape Town_2.5	0.012	0.012	0.005
Cape Town_10	0.095	0.095	0.018
Cape Town_14.3	0.130	0.129	0.020
Cape Town_25	0.374	0.372	0.027
Cape Town_100	9.673	9.667	0.158
Cape Town_143	15.376	15.359	0.204
Cape Town_250	24.233	24.214	0.238
Pointe Noire_2.5	0.000	0.000	0.000
Pointe Noire_10	0.000	0.000	0.000
Pointe Noire_14.3	0.000	0.000	0.000
Pointe Noire_25	0.000	0.000	0.000
Pointe Noire_100	0.000	0.000	0.000
Pointe Noire_143	0.000	0.000	0.000
Pointe Noire_250	0.000	0.000	0.000
Buenos Aires_2.5	0.447	0.449	0.034
Buenos Aires_10	2.328	2.333	0.089
Buenos Aires_14.3	2.303	2.307	0.088
Buenos Aires_25	1.499	1.501	0.064
Buenos Aires_100	0.000	0.000	0.000
Buenos Aires_143	0.000	0.000	0.000
Buenos Aires_250	0.210	0.210	0.015
Rio de Janeiro_2.5	0.000	0.000	0.000
Rio de Janeiro_10	0.000	0.000	0.000
Rio de Janeiro_14.3	0.000	0.000	0.000
Rio de Janeiro_25	0.010	0.010	0.003
Rio de Janeiro_100	2.462	2.465	0.078
Rio de Janeiro_143	5.435	5.441	0.122
Rio de Janeiro_250	10.218	10.227	0.162
Salvador_2.5	0.000	0.000	0.000
Salvador_10	0.004	0.004	0.001
Salvador_14.3	0.018	0.019	0.004
Salvador_25	0.085	0.085	0.012
Salvador_100	0.456	0.456	0.035
Salvador_143	0.415	0.415	0.030
Salvador_250	0.752	0.751	0.031
Recife_2.5	0.000	0.000	0.000
Recife_10	0.000	0.000	0.000
Recife_14.3	0.000	0.000	0.000
Recife_25	0.000	0.000	0.000
Recife_100	0.002	0.002	0.001
Recife_143	0.008	0.008	0.003
Recife_250	0.713	0.712	0.034
Montevideo_2.5	0.219	0.219	0.021
Montevideo_10	0.939	0.943	0.051
Montevideo_14.3	1.386	1.392	0.064
Montevideo_25	2.983	2.990	0.091
Montevideo_100	9.539	9.541	0.162
Montevideo_143	14.330	14.330	0.192
Montevideo_250	24.550	24.556	0.241

Table B.9: Probabilities calculated for *van Sebille et al. (2015)* from the quadratic distribution when considering the entire 5-year simulation.

	van Sebille et al. (2015) - 2.5 yrs	Bootstrap Mean	Bootstrap St Dev
Luanda_2.5	0.000	0.000	0.000
Luanda_10	0.000	0.000	0.000
Luanda_14.3	0.000	0.000	0.000
Luanda_25	0.000	0.000	0.000
Luanda_100	0.000	0.000	0.000
Luanda_143	0.000	0.000	0.000
Luanda_250	0.000	0.000	0.000
Benguela_2.5	0.000	0.000	0.000
Benguela_10	0.000	0.000	0.000
Benguela_14.3	0.000	0.000	0.000
Benguela_25	0.000	0.000	0.000
Benguela_100	0.000	0.000	0.000
Benguela_143	0.000	0.000	0.000
Beguela_250	0.027	0.027	0.008
Cape Town_2.5	0.012	0.012	0.005
Cape Town_10	0.095	0.095	0.017
Cape Town_14.3	0.130	0.130	0.020
Cape Town_25	0.372	0.372	0.027
Cape Town_100	9.478	9.477	0.165
Cape Town_143	15.103	15.101	0.209
Cape Town_250	23.880	23.883	0.250
Pointe Noire_2.5	0.000	0.000	0.000
Pointe Noire_10	0.000	0.000	0.000
Pointe Noire_14.3	0.000	0.000	0.000
Pointe Noire_25	0.000	0.000	0.000
Pointe Noire_100	0.000	0.000	0.000
Pointe Noire_143	0.000	0.000	0.000
Pointe Noire_250	0.000	0.000	0.000
Buenos Aires_2.5	0.287	0.287	0.027
Buenos Aires_10	1.649	1.649	0.077
Buenos Aires_14.3	1.673	1.672	0.078
Buenos Aires_25	1.048	1.047	0.054
Buenos Aires_100	0.000	0.000	0.000
Buenos Aires_143	0.000	0.000	0.000
Buenos Aires_250	0.196	0.196	0.015
Rio de Janeiro_2.5	0.000	0.000	0.000
Rio de Janeiro_10	0.000	0.000	0.000
Rio de Janeiro_14.3	0.000	0.000	0.000
Rio de Janeiro_25	0.006	0.006	0.003
Rio de Janeiro_100	2.037	2.035	0.070
Rio de Janeiro_143	4.913	4.909	0.110
Rio de Janeiro_250	9.842	9.842	0.160
Salvador_2.5	0.000	0.000	0.000
Salvador_10	0.004	0.004	0.001
Salvador_14.3	0.018	0.018	0.004
Salvador_25	0.083	0.083	0.012
Salvador_100	0.452	0.451	0.035
Salvador_143	0.412	0.411	0.030
Salvador_250	0.752	0.753	0.033
Recife_2.5	0.000	0.000	0.000
Recife_10	0.000	0.000	0.000
Recife_14.3	0.000	0.000	0.000
Recife_25	0.000	0.000	0.000
Recife_100	0.002	0.002	0.001
Recife_143	0.008	0.008	0.003
Recife_250	0.713	0.713	0.033
Montevideo_2.5	0.217	0.218	0.021
Montevideo_10	0.904	0.903	0.050
Montevideo_14.3	1.322	1.322	0.063
Montevideo_25	2.805	2.806	0.091
Montevideo_100	8.565	8.568	0.167
Montevideo_143	12.702	12.702	0.189
Montevideo_250	22.306	22.306	0.233

Table B.10: Probabilities calculated for *van Sebille et al. (2015)* from the quadratic distribution when considering only the first 2.5 years of the simulation.